

**ICHTHOLOGY OF THE MARINE K-PG INTERVAL:
ENDOBENTHIC RESPONSE TO A LARGE-SCALE
ENVIRONMENTAL DISTURBANCE**

A Thesis
Submitted to the
Temple University Graduate Board

In Partial Fulfillment
of the Requirement for the Degree
MASTER OF SCIENCE
GEOLOGY

by
Logan A. Wiest
May 2014

Dr. Ilya V. Buynevich, Thesis Advisor

Dr. Dennis O. Terry, Jr.

Dr. David E. Grandstaff

ABSTRACT

Most major Phanerozoic mass extinctions induced permanent or transient changes in ecological and anatomical characteristics of surviving benthic communities. Many infaunal marine organisms produced distinct suites of biogenic structures in a variety of depositional settings, thereby leaving an ichnological record preceding and following each extinction. This study documents a decrease in burrow size in *Thalassinoides*-dominated ichnoassemblages across the Cretaceous-Paleogene (K-Pg) boundary in shallow-marine sections along the Atlantic Coastal Plain (Walnridge Farm, Rancocas Creek, and Inversand Quarry, New Jersey) and the Gulf Coastal Plain (Braggs, Alabama and Brazos River and Cottonmouth Creek, Texas). At New Jersey sites, within a regionally extensive ichnoassemblage, *Thalassinoides* ichnospecies (isp.) burrow diameters (D_{Th}) decrease abruptly by 26-29% (mean K=15.2 mm, mean Pg=11.2 mm; n=1767) at the base of the Main Fossiliferous Layer (MFL) or laterally equivalent horizons. The MFL has been previously interpreted as the K-Pg boundary based on last occurrence of Cretaceous marine reptiles, birds, and ammonites, as well as iridium anomalies and associated shocked quartz. Across the same event boundary at Braggs, Alabama, D_{Th} of simple maze *Thalassinoides* structures from recurring depositional facies decrease sharply by 22% (mean K=13.1 mm, mean Pg=10.2 mm; n=26). Similarly, at the Cottonmouth Creek site, Texas, *Thalassinoides* isp. occurring above the previously reported negative $\delta^{13}C$ shift and the first occurrence of Danian planktonic foraminifera are 17% smaller in diameter (mean K=21.5 mm, mean Pg=17.9 mm; n=53) than those excavated and filled prior to deposition of a cross-bedded, ejecta-bearing sandstone complex commonly interpreted as the Chicxulub 'event deposit'. At both of these impact-

proximal regions, the Cretaceous and Paleogene burrows were preserved in similar lithologies, suggesting that a reduction in size cannot be attributed to sedimentological factors. At all localities, up-section trends in D_{Th} are statistically significant ($\alpha < 0.05$; non-parametric Kruskal-Wallis test). Using the burrow diameter as a proxy for tracemaker body size, a reduction in D_{Th} above the K-Pg boundary likely reflects dwarfing within the post-extinction community of decapod crustaceans. Dwarfing during the early recovery stages of the end-Cretaceous mass extinction, as recorded by ichnofossils, occurred within glauconite-producing (New Jersey), carbonate (Alabama), and siliciclastic (Texas) depositional environments and appears to be widespread. Because this ichnological signal appears to be a general phenomenon across the crisis interval, trace-fossil analysis provides a potential *in-situ* field method for constraining and correlating the stratigraphic position of the K-Pg and other extinction events, particularly in the absence of other macroscopic, microscopic, and geochemical indicators.

Whereas overprinting of the original marine ichnofabric by morphologically similar continental traces is not a concern in lithified sections of Alabama and Texas, such an occurrence must be considered within unconsolidated sections. Within the Hornerstown Formation of New Jersey, a pervasive *Thalassinoides* framework contains traces of burrowing bees and wasps. Due to their penetration of up to 1 m, excavations just beyond the weathering front are insufficient for exposing the original marine ichnofabric. Insect burrow diameters (7-25 mm) are within the range of *Thalassinoides* traces (4-31 mm), exhibit occasional branching, and lack of ornamentation (bioglyphs) on

the burrow walls. Therefore neither size nor gross morphology are adequate for distinguishing these widely diachronous and unrelated ichnites, especially when the insect burrows have been filled. However, the presence of backfill menisci and a beige clay halo help distinguish the ancient marine burrows, whereas highly oxidized fill and the occurrence of a terminal brooding chamber are diagnostic of modern insect burrows.

ACKNOWLEDGMENTS

The list of individuals that have taught, assisted and/or encouraged me throughout this project is very long, and if I forgot to include anyone, I apologize for my oversight.

First and foremost I would like to thank my thesis advisor, Ilya Buynevich, for providing the freedom and support to explore my research interests. The work contained within this thesis reflects only a portion of the time and effort that Ilya has devoted to developing my abilities and preparing me for a career in geology.

A substantial portion of the prospecting, digging, and data collection that this study required is attributed to Zach Maza's perseverance for this project. In no way could I ever ask for a more reliable and hard-working field and lab partner. His contribution to this study exceeded all expectations.

Several other individuals contributed to the field work in New Jersey. This includes Robbie Horner, Eve Eisemann, Zack Grimmes, and Jeff Moore. Their assistance is greatly appreciated.

I would also like to express my great appreciation and respect to Dennis Terry Jr. and David Grandstaff. They have dedicated countless hours to assisting me with this project, teaching me many different aspects of how our dynamic world has changed through time, and showing me how we can access the record through ancient archives.

I would also like to thank the rest of the faculty from the TU Geology Department. In particular, Jonathan Nyquist and Alexandra Davatzes were always insightful and helpful when I approached them for ideas or direction.

I must note my gratitude for Shelah Cox and Jim Ladd. The support that they provide regularly exceeds the call of duty, and Shelah's kindness never fails to make the day better.

I would also like to acknowledge the individuals who have significantly contributed to my education of the K-Pg boundary and mass extinction through discussions and/or collaboration. This includes Kenneth Lacovara, Matthew Garb, William Gallagher, Kenneth Miller, Tony Ekdale, Richard Twitchett, and Malcolm Hart. Their discussions and insight for this project are greatly valued.

Trying to become a better teacher and researcher certainly requires a team effort. For this I am greatly thankful for my fellow peers and graduate students who are eager to engage in discussions ranging from teaching methods to deep time. In particular this includes, but is not limited to, Bill Lukens, Chris Oest, Stephen Peterson, Steven Booty, Jesse Thornburg, Justin Roth, and Nick 'The Dog' Swartz.

Hungerford & Terry Inc., Drexel University, Richard Meirs, Flying W Airport, and the owners and staff of the Mullinax Ranch graciously provided access to the field sites. Funding for research and travel was provided by Temple University and the Geological Society of America.

Last but not least, I must also note that none of this fun and interesting stuff would be possible for me if it weren't for the unconditional support and encouragement by Katie.

TABLE OF CONTENTS

	Page
ABSTRACT.....	i
ACKNOWLEDGMENTS.....	iv
LIST OF FIGURES.....	ix
LIST OF TABLES.....	x
CHAPTER 1: ICHNOLOGICAL SIGNAL OF THE K-PG EVENT, NJ	
1.1 Abstract.....	1
1.2 Introduction.....	2
1.3 Geologic Setting.....	3
1.3.1 Inversand Quarry.....	4
1.3.2 Rancocas Creek.....	6
1.3.3 Walnridge Farm.....	7
1.4 Methods.....	7
1.5 Results.....	9
1.5.1 Trace Morphology.....	9
1.5.2 <i>Thalassinoides</i> Diameters.....	10
1.5.3 Ichnofabric.....	13
1.6 Discussion.....	13
1.7 Conclusions.....	17
CHAPTER 2: ICHNOLOGICAL SIGNAL OF THE K-PG EVENT, BRAGGS, AL, & BRAZOS RIVER, TX	
2.1 Abstract.....	22
2.2 Introduction.....	23
2.3 Geologic Setting.....	26
2.3.1 Braggs, Alabama.....	26
2.3.2 Brazos River And Cottonmouth Creek, Texas.....	27
2.4 Methods.....	30
2.5 Results & Discussion.....	31
2.5.1 Braggs, Alabama.....	31
2.5.2 Brazos River And Cottonmouth Creek, Texas.....	32
2.6 Conclusions.....	37
CHAPTER 3: OVERPRINTING OF K-PG <i>THALASSINOIDES</i> BY BURROWING INSECTS, SEWELL, NJ	
3.1 Abstract.....	38
3.2 Introduction.....	38
3.3 Geologic Setting.....	40
3.4 Methods.....	40
3.5 Results.....	41
3.6 Discussion.....	43
3.7 Conclusions.....	49
REFERENCES.....	50

APPENDICES

APPENDIX A. D_{Th} AND STRATIGRAPHIC POSITION AT INVERSAND.....67
APPENDIX B. D_{Th} AND STRATIGRAPHIC POSITION AT RANCOCAS.....98
APPENDIX C. D_{Th} AND STRATIGRAPHIC POSITION AT WALNRIDGE.....115
APPENDIX D. D_{Th} AND BED # AT BRAGGS.....124
APPENDIX E. D_{Th} AND UNIT AT BRAZOS RIVER / COTTONMOUTH CREEK..125

LIST OF FIGURES

1.1 Location map of New Jersey study sites.....	5
1.2 Stratigraphic nomenclature and placement of K-Pg boundary.....	8
1.3 <i>Thalassinoides</i> morphology and fill characteristics.....	11
1.4 Burrow fragments recovered from the MFL.....	12
1.5 D_{Th} across the K-Pg boundary at Inversand, Rancocas, and Walnridge.....	13
1.6 Schematic diagram of events across the K-Pg boundary.....	20
2.1 Location map of the Gulf Coastal Plain study sites.....	25
2.2 Stratigraphic nomenclature and traces at Braggs.....	28
2.3 Stratigraphic nomenclature and traces at Brazos.....	29
2.4 D_{Th} across the K-Pg boundary at Inversand, Braggs, and Brazos.....	36
3.1 Location map of Inversand Quarry, New Jersey.....	42
3.2 Modern continental trace fossils.....	45
3.3 K-Pg marine trace fossils.....	46
3.4 Weathering of continental and marine traces.....	47
3.5 Marine and continental burrow diameters.....	48

LIST OF TABLES

1.1 Statistical results of D_{Th} across the K-Pg boundary in New Jersey.....	18
1.2 Ichnofabric index values at Inversand, Rancocas, and Walnridge.....	19
2.1 Statistical results of D_{Th} at Braggs, Brazos, and Inversand.....	35

CHAPTER 1: ICHNOLOGICAL SIGNAL OF THE K-PG EVENT, NEW JERSEY

Manuscript in revision, PALAIOS (Wiest et al., accepted)

1.1 Abstract

Thalassinoides isp. burrow morphology, ichnofabric, and diameters were compared across the Cretaceous-Paleogene (K-Pg) boundary interval at three localities along the New Jersey coastal plain. Within this regionally extensive ichnoassemblage, burrow diameters decrease abruptly by 26-29% (n=1767) at the base of the Main Fossiliferous Layer (MFL) or laterally equivalent horizons. The MFL has been previously interpreted as the K-Pg boundary based on the last occurrence of Cretaceous marine reptiles, birds, and ammonites, as well as iridium anomalies and associated shocked quartz. The statistical parameters of burrow size exhibit a negative shift, which indicates that the changes are the result of a directional reduction in diameter, rather than an artifact of decreased variance. As a proxy for the size of the tracemaker, a change in burrow diameter indicates a decrease in thalassinid crustacean body size. We interpret this shift as dwarfing within the endobenthic community as detrital food sources became scarce following the end-Cretaceous mass extinction. The occurrence of active fill in some Danian burrows is also consistent with a change in feeding strategy. Despite the difference in burrow size, there is no change in framework geometry. Ichnofabric indices generally increase up-section at each site across the K-Pg, indicating a regional reduction in sedimentation rate, which is supported by a gradual increase in glauconite maturity.

Overall, the ichnological evidence at these localities suggests that a prolonged period of negative feedback followed a short-term positive endobenthic response to the extinction.

1.2 Introduction

The mass extinction at the end of the Cretaceous Period was one of the most dramatic biotic crises of the Phanerozoic. However, the ability to burrow and scavenge allowed primitive, ecologically generalized organisms to preferentially survive this event (Van Valen, 1994; Sheehan et al., 1996; Schweitzer and Feldmann, 2005). The coastal plain of New Jersey contains bioturbated, glauconite-rich marine sections that span the Cretaceous-Paleogene (K-Pg) boundary (Fig. 1.1). Over the past several decades, a number of studies have focused on the geochemistry, sedimentology, and particularly the paleontology across the K-Pg boundary in New Jersey (e.g., Baird, 1967; Minard et al., 1969; Gallagher, 1984, 1990, 1993, 2003, 2012; Gallagher et al., 1986, 2003, 2012; Self-Trail and Bybell, 1995; Kennedy and Cobban, 1996; Staron et al., 2001; Olsson et al., 2002; Landman et al., 2004, 2007; Miller et al., 2010; Obasi et al., 2011). However, with the exception of the Bass River core (Fig. 1.1, site B; Olsson et al., 1997; Miller et al., 2010), endobenthic bioturbation may have masked, translocated, or diffused diagnostic criteria used for stratigraphic placement of the K-Pg boundary, including shocked quartz, age-specific nannofossils, and geochemical anomalies (Ir, $\delta^{13}\text{C}$; Self-Trail and Bybell, 1995; Obasi et al., 2011; Gallagher, 2012; Keller, 2012).

Although bioturbation has complicated many attempts to precisely place the K-Pg boundary in marine sections, we utilize the *in situ* context of the biogenic structures to

help understand the depositional history and effect of subsequent reworking on the K-Pg interval of New Jersey, as well as provide insight into the endobenthic ecological response to the extinction event (Ekdale and Bromley, 1984; Savrda, 1993; Ekdale and Stinnesbeck, 1998; Rodríguez-Tovar, 2005; Morrow and Hasiotis, 2007; Wroblewski, 2008). The aim of this paper is to compare the ichnofabric index, framework geometry, sedimentary fill, and the size of burrows across the K-Pg boundary at three sites in New Jersey in order to: (1) assess the depth and degree of bioturbation as a measure of sediment reworking, and (2) to document a regionally extensive shift in burrow diameter across the event boundary.

1.3 Geologic Setting

The Upper Cretaceous (Maastrichtian) and Lower Paleogene (Danian) strata along the New Jersey coastal plain consist of slightly southeastward-dipping, unconsolidated, glauconite-rich sequences which were deposited in a mid-to-inner-shelf environment during several transgressive-regressive cycles (Fig. 1.1; Gallagher, 1993; Bennington, 2003; Miller et al., 2004, 2010; Obasi et al., 2011). At Inversand and Rancocas (Fig. 1.1, sites I and R), the Upper Cretaceous Navesink Formation is an approximately 3-m-thick olive-gray to dusky brown clayey-glauconitic sand (Minard et al., 1969; Owens et al., 1970) deposited on the inner-shelf (Wolfe, 1977; Gallagher, 1993). The overlying Hornerstown Formation is a 5.5-m-thick fine-to-medium-grained, grayish olive green glauconitic sand (Minard et al., 1969) deposited on the mid-to-outer shelf (Wolfe, 1977; Gallagher, 1993). The Hornerstown Formation contains Upper

Cretaceous invertebrate and vertebrate fossils near its base, but otherwise contains Danian invertebrate remains. At Walnridge Farm (Fig. 1.1, site W), the Hornerstown Formation overlies the Upper Cretaceous New Egypt Formation, which is a massive, dark gray-brown glauconitic clayey sand up to 27 m in thickness (Olsson, 1963). The New Egypt Formation is interpreted as an inner-shelf deposit and a lateral facies equivalent of the Navesink Formation (Koch and Olsson, 1977; Wolfe, 1977; Gallagher, 1993). The contact between the Hornerstown and underlying formations has been variously interpreted as a disconformity (e.g. Koch and Olsson, 1977; Landman et al, 2007), minor paraconformity (Baird, 1967; Gallagher et al., 1986; Gallagher, 1993, 2003), and a lowstand sequence boundary (Gallagher, 2003; Miller et al., 2004).

1.3.1 Inversand Quarry

The Inversand Quarry at Sewell, New Jersey (39° 45'45" N, 75° 7'38" W) (Fig.1.1, site I) is a glauconite pit within the Upper Navesink and Hornerstown Formations that preserves one of the best exposed K-Pg sections along the Atlantic Coastal Plain (Fig. 1.2). The quarry is well known for the Main Fossiliferous Layer (MFL), a ca. 10-cm-thick bonebed that contains remains of Late Cretaceous vertebrate fossils, including mosasaurs, fish, crocodiles, turtles, and birds (Gallagher, 1993). These are occasionally articulated and associated, and mixed with Danian microfossils (e.g., Gallagher et al., 1986, 2003; Gallagher, 1990, 1993, 2003; Self-Trail and Bybell, 1995; Landman et al., 2004, 2007). The MFL is located in the basal Hornerstown Formation, approximately 20 cm above the Navesink-Hornerstown contact (Fig. 1.2; Obasi et al., 2011). The MFL has been interpreted as an assemblage of Cretaceous fossils reworked

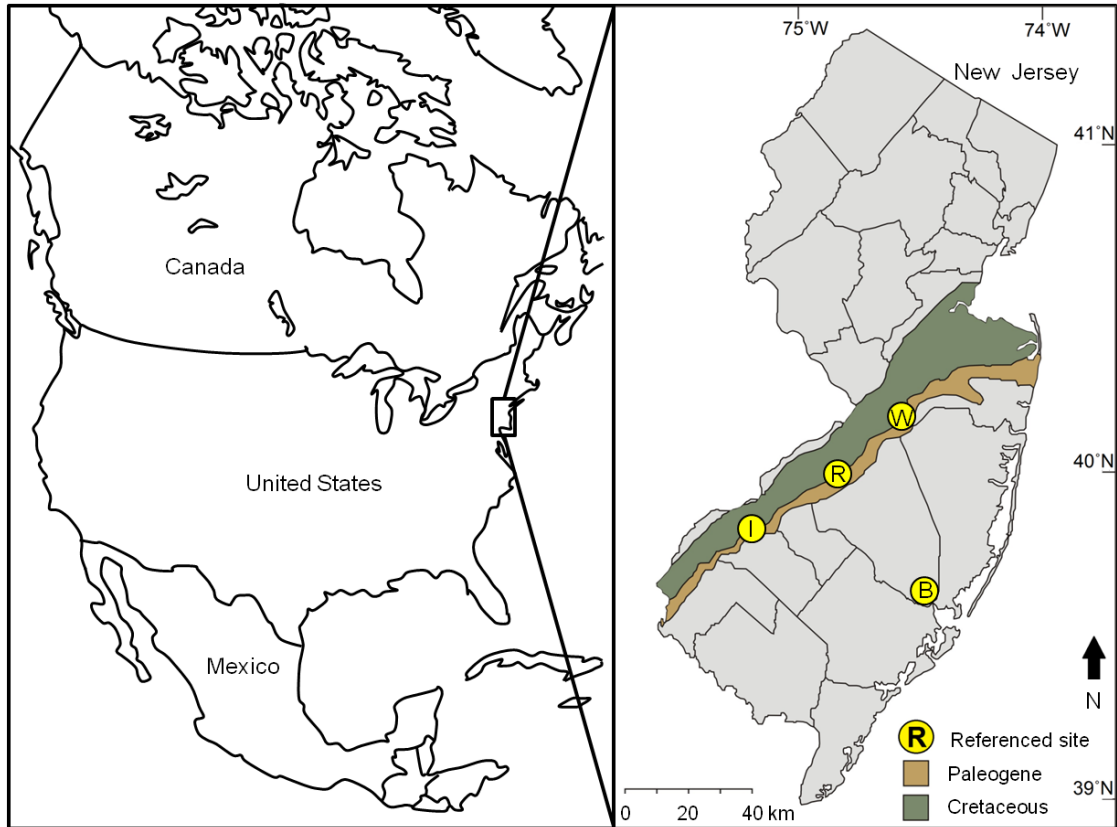


Figure 1.1 – Study localities across the New Jersey coastal plain. I = Inversand Quarry, Sewell; R = Rancocas Creek, Medford; W = Walnridge Farm, Hornerstown; B = Bass River, New Gretna. Figure modified from Obasi et al. (2011).

into Paleogene sediments (e.g., Landman et al., 2007), a condensed section (Kennedy and Cobban, 1996), a concentration resulting from intense bioturbation through the K-Pg boundary (Gallagher, 1993), and a thanatocoenosis (Gallagher, 2003, 2012; Obasi et al., 2011). Recently, shocked quartz and elevated Ir levels have been found associated with the MFL (Obasi et al., 2011; Gallagher, 2012). The K-Pg boundary at Inversand has been variously placed at the Navesink-Hornerstown lithologic contact (Fig. 1.2, position A; Minard et al., 1969, 1976; Owens et al., 1970; Self-Trail and Bybell, 1995; Kennedy and Cobban, 1996), at the base of or within the MFL (Fig. 1.2, position B; Koch and Olsson, 1977; Hope, 1999; Gallagher, 2002, 2003, 2012; Obasi et al., 2011), and above the MFL within the Hornerstown Formation (Fig. 1.2, position C; Olsson, 1963; Parris, 1974; Staron et al., 2001).

1.3.2 Rancocas Creek

The Rancocas Creek locality at Medford, New Jersey (39° 55'46" N, 74° 48'23" W) (Fig.1.1, site R) is located along a cutbank on the western side of Rancocas Creek just south of the airstrip at Flying W Airport. This locality also contains a fossil-rich layer, approximately 20 cm above the Navesink-Hornerstown contact that contains the last known occurrence of Cretaceous vertebrate and invertebrate body fossils (MFL equivalent) and is tentatively considered the K-Pg boundary (Koch and Olsson, 1977; Hope, 1999).

1.3.3 Walnridge Farm

The Walnridge Farm exposure at Cream Ridge, New Jersey (40° 6'22" N, 74° 31'32" W) (Fig. 1.1, site W) sits along a small tributary of Crosswicks Creek. Marl pits in the New Egypt Formation at and around the Walnridge (Meirs' Farm) site have been an important historic source of Cretaceous fossils, including plesiosaurs, mosasaurs, and ammonites (e.g., Gallagher et al., 2012). Previous coring at this site revealed a modest iridium anomaly of 0.5 ppb within a clay clast at the New Egypt-Hornerstown contact, thus placing the K-Pg boundary at the formational contact (Miller et al., 2010).

1.4 Methods

At the three localities, a total of nineteen fresh exposures were excavated across the K-Pg boundary, as previously interpreted from paleontological, sedimentological, and geochemical studies (Gallagher, 1993, 2012; Hope, 1999; Staron et al., 2001; Miller et al., 2010; Obasi et al., 2011). Excavations exposed unaltered sections beyond the influence of surficial weathering and modern burrowing organisms (Hasiotis and Bown, 1992; Hasiotis, 2002; Wiest and Buynevich, in review). Burrows were examined for architectural and surficial morphology, as well as fill characteristics and diagenetic features. A Dino-Lite digital field microscope was used for *in situ* imaging of key burrow attributes. Since ichnofossils occurring below and above the K-Pg boundary are morphologically similar (Fig. 1.3A-B), we use the inner burrow diameter as a proxy for tracemaker body size (Twitchett and Barras, 2004). The minimum inner diameters (D_{Th}) of shafts and tunnels were measured with a digital vernier caliper to the nearest 0.01 mm, with the distance from enlarged junctions taken into account to ensure the consistency of

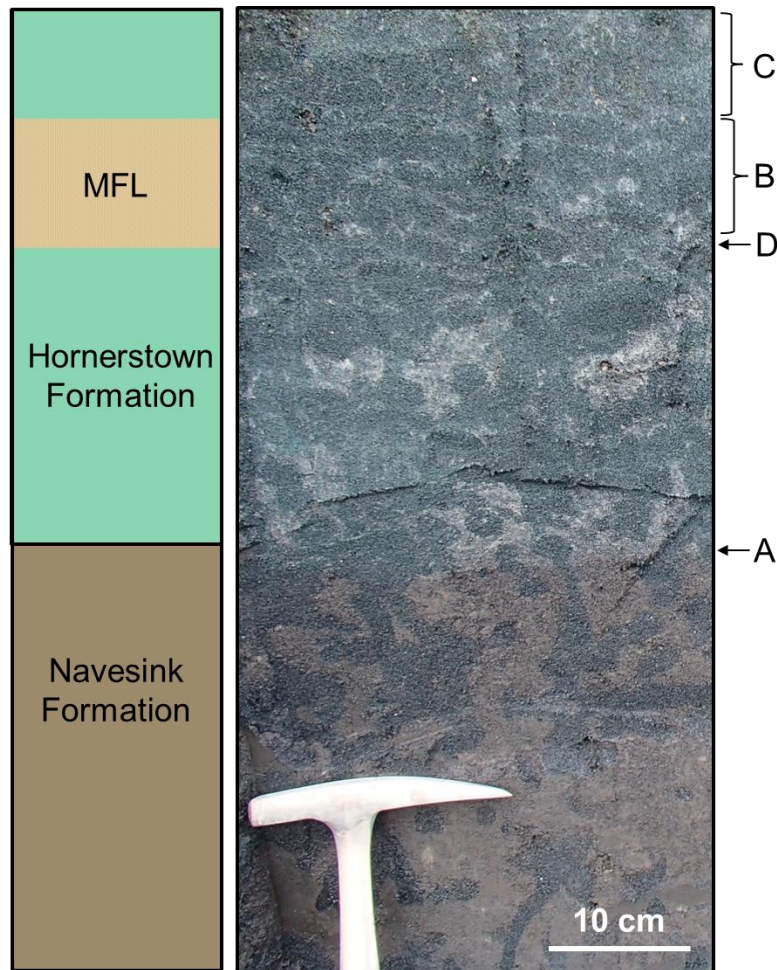


Figure 1.2 – Lithologic units and various interpreted K-Pg boundaries at Inversand Quarry. MFL represents stratigraphic placement of the Main Fossiliferous Layer. A = interpreted stratigraphic position of K-Pg boundary by Minard et al. (1969, 1976), Owens et al. (1970), Self-Trail and Bybell (1995), and Kennedy and Cobban (1996); B = interpreted stratigraphic position of K-Pg boundary by Koch and Olsson (1977), Hope (1999), and Gallagher (2002, 2003); C = interpreted stratigraphic position of K-Pg boundary by Olsson (1963), Parris (1974), and Staron et al. (2001); D = interpreted stratigraphic position of K-Pg boundary by Obasi et al. (2011) and Gallagher (2012).

measurements. Measurements were grouped into 5-10 cm stratigraphic intervals based on sample number, and the mean D_{Th} , standard deviation, and standard error were calculated. Differences between D_{Th} from below and above the K-Pg boundary were evaluated with a non-parametric Kruskal-Wallis test (Davis, 1986; Smith et al., 2009). Ichnofabric indices were evaluated using a semi-quantitative field method proposed by Miller and Smail (1997).

1.5 Results

1.5.1 Trace Morphology

The *in situ* ichnoassemblage at each measured section is composed of monospecific *Thalassinoides* isp. identified by their characteristic boxwork morphology and absence of biogenic ornamentation, such as pelleted lining or sculpturing (bioglyphs) along the walls (Fig. 1.3A). Burrows in the top 2 m of the underlying New Egypt/Navesink Formations are most readily recognized by their dark bluish-gray glauconite fill derived from the Hornerstown Formation (Horner et al., 2013), which contrasts with the dusky brown glauconitic-clay matrix and indicates that some burrows penetrated to a depth of approximately 2 m (Fig. 1.3B; Wiest et al., 2012a). These traces are dominated by vertical to sub-vertical shafts that branch downward into a network of horizontal to slightly inclined tunnels. Traces within the overlying Hornerstown Formation also form a horizontal boxwork with characteristic T, X, and Y-junctions (Fig. 1.3A). Branching was observed in all orientations but is most common in bedding-plane exposures. Burrows higher in the Hornerstown Formation are easily recognized by their

nearly pure glauconitic fill, as well as a beige clay halo that is more prominent on the outside of the burrow wall and diffuses outward into the surrounding sandy matrix (Figs. 1.3A, C-F). A few burrows (< 5%) above the K-Pg boundary contain backfill menisci in both shafts and tunnels (Fig. 1.3C-D), but menisci were not observed at any junction points.

Sparse fragments of lithified burrows (*Skolithos* isp.?) were recovered from the unconsolidated sediments within the lower portion of the MFL (Fig. 1.4). These fragments do not contain a preferential orientation, nor do they exhibit any indication of branching. A few (<10%) of the trace segments preserve smooth inner walls (Fig. 1.4E), whereas the majority display a coarse lining containing large glauconite grains.

1.5.2 *Thalassinoides* Diameters

D_{Th} values, grouped into 5 to 10 cm stratigraphic intervals, are shown in Fig. 1.5. Burrow diameters decrease at the stratigraphic position of the MFL and the inferred K-Pg boundary of Miller et al. (2010), Obasi et al. (2011), and Gallagher et al. (2012). At all sites, most traces below the MFL and/or iridium anomaly have diameters ranging from 7 to 27 mm, with rare values of <5 mm and >30 mm (Appendix 1-3). Burrow diameters within the overlying strata generally range from 4 to 18 mm, with occasional traces measuring less than 3 mm and greater than 20 mm. Based on the non-parametric Kruskal-Wallis test, burrow diameters are significantly different above and below the MFL, as well as above and below the previously reported iridium anomalies (Table 1.1). Since the lithified, sparse *Skolithos* fragments found within the MFL at Inversand are structurally

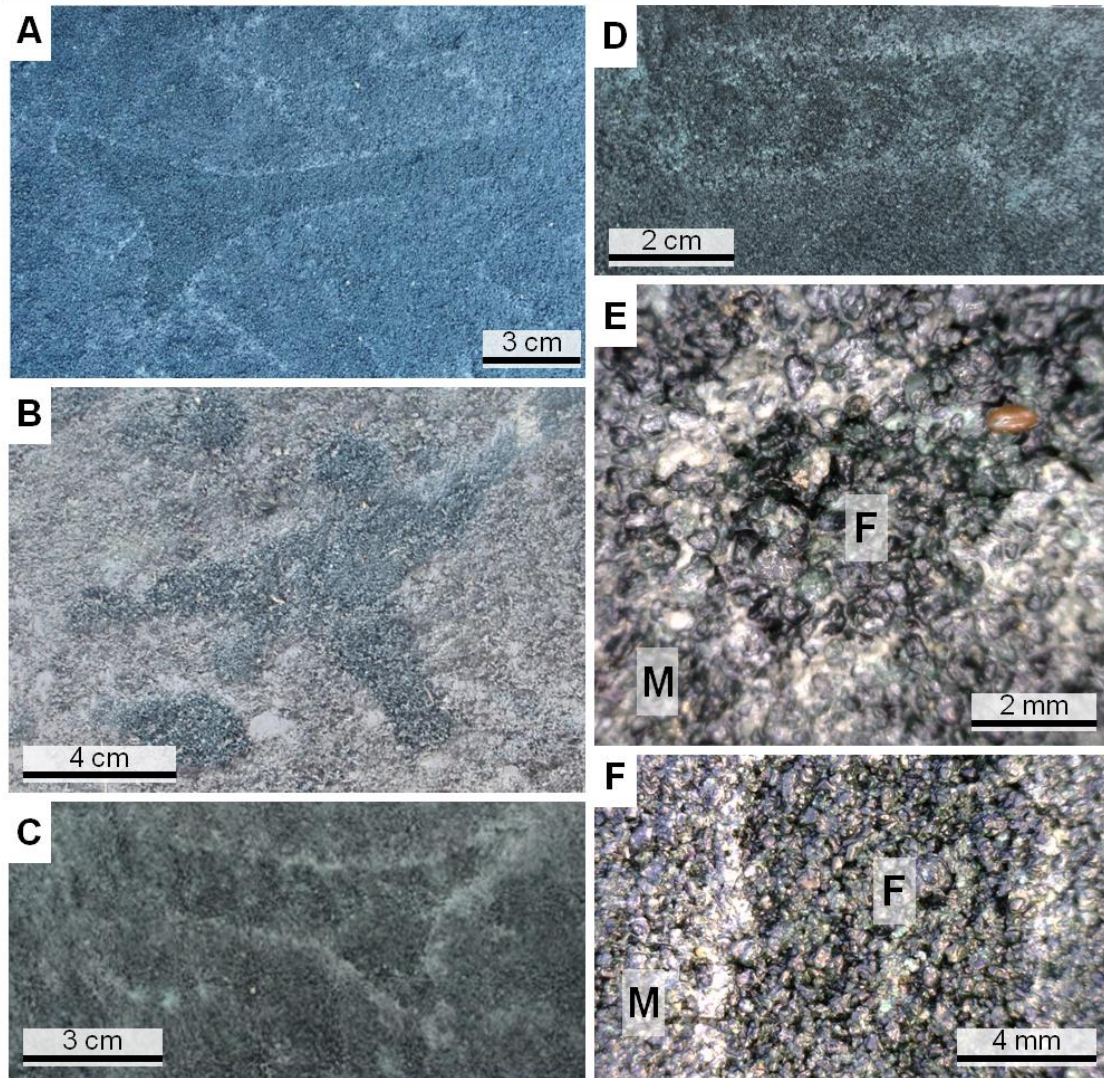


Figure 1.3 – A) Bedding exposures of Y-junctions characteristic of *Thalassinoides* in the Hornerstown Formation and B) the underlying Navesink Formation at Inversand Quarry. C) Bedding exposures of actively filled tunnels above the K-Pg boundary and D) at/near the K-Pg boundary at Inversand Quarry. E) *In situ* glauconite grains and a beige-clay halo surrounding longitudinal cross-section of tunnel and F) transverse cross-section of shaft in the Hornerstown Formation at Inversand; F and M = burrow fill and surrounding matrix, respectively.

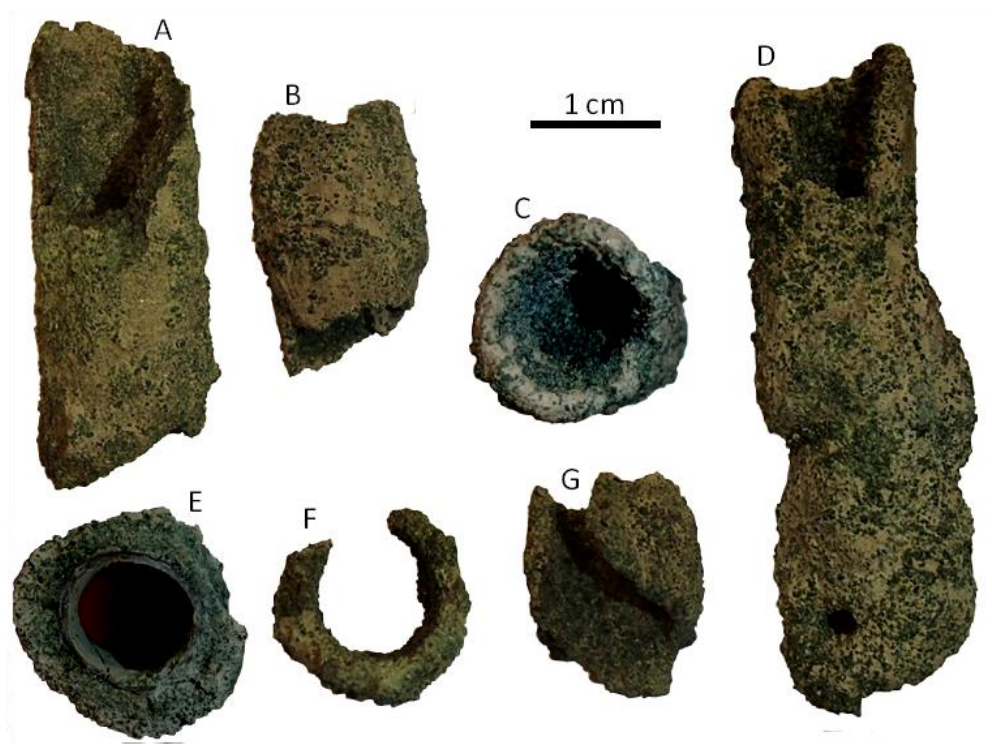


Figure 1.4 – Examples of lithified burrow fragments recovered from the MFL at Inversand showing internal and external features. Note the smooth clay lining in specimen E.

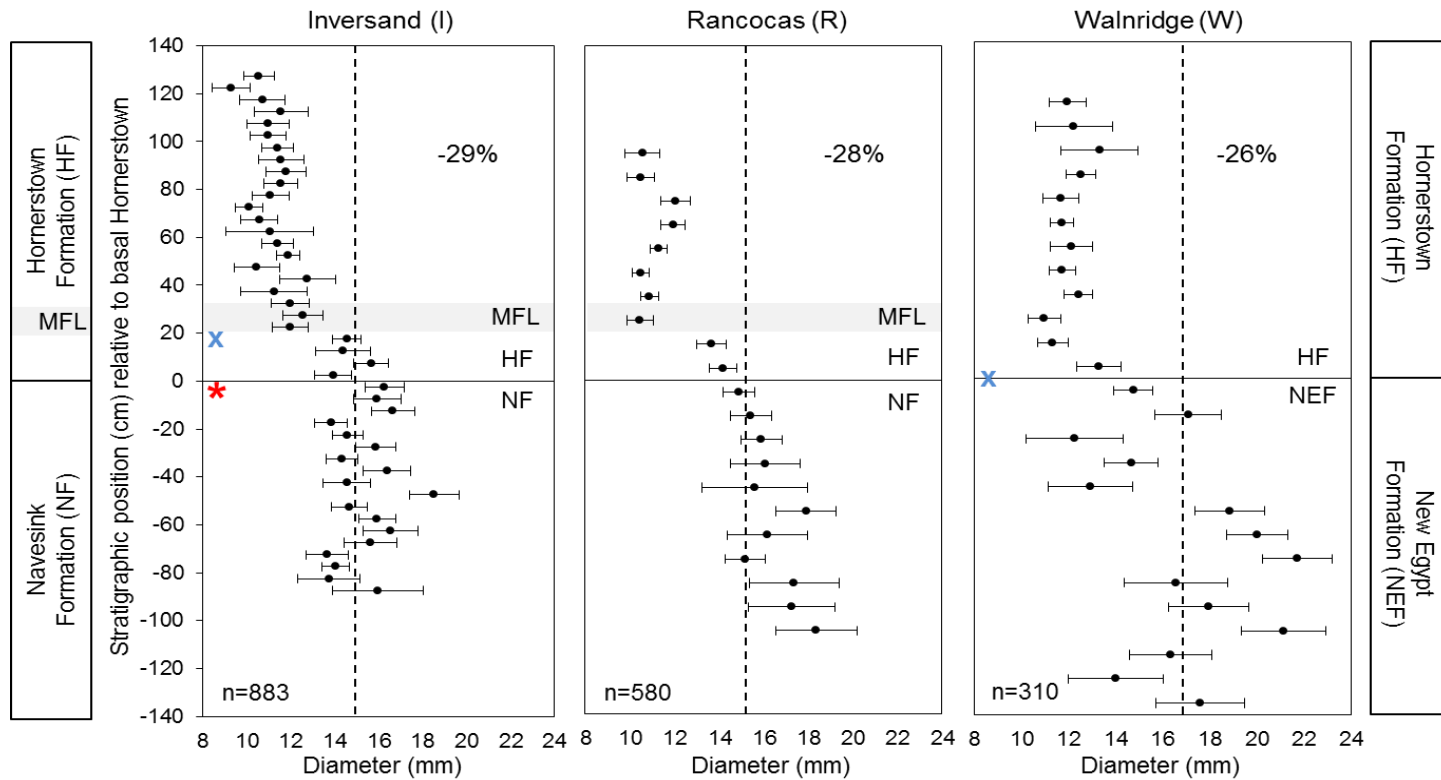


Figure 1.5 – *Thalassinoides* burrow diameters and percent changes in mean size above the base of the MFL at Inversand and Rancocas, and above the iridium anomaly (Miller et al., 2010) at Walnridge. Black circles = mean diameter; horizontal bars = one standard error for diameters binned at 5 to 10 cm stratigraphic intervals; and dashed vertical lines fitted to mean burrow diameter below the MFL and/or iridium anomaly; gray area = Main Fossiliferous Layer; X = location of elevated iridium; asterisk = shocked quartz within burrow (Obasi et al., 2011), n = number of burrows measured at each locality. Stratigraphic column on the right represents the Walnridge locality whereas the column on the left represents Inversand and Rancocas.

and morphologically distinct from the *Thalassinoides* burrows, the inner diameters of these traces were not included in the statistical analysis.

1.5.3 Ichnofabric

The degree of bioturbation across the K-Pg boundary was assessed using the ichnofabric index of Miller and Smail (1997) at 10-cm stratigraphic intervals (Table 1.2; see Miller and Smail, 1997 for detailed discussion on methods). An ichnofabric index scale of 1-5 was utilized, with 1 for absence of bioturbation and 5 representing little to no physical sedimentary structures (Droser and Bottjer, 1986). Trends in ichnofabric indices at each site reveal a general increase in bioturbation across the K-Pg boundary (Table 1.2). Isolated and partially overlapping burrows occurring in the base of each measured section show an increase in bioturbation intensity up-section until complete or nearly complete disturbance 20–40 cm above the K-Pg boundary (Wiest et al., 2012b). At approximately 1.6 m above the base of the Hornerstown Formation, bioturbation becomes so intense that individual burrows can no longer be differentiated.

1.6 Discussion

Based on the interpreted paleoenvironmental context and modern analogs of thalassinidean burrows, the *Thalassinoides* tracemakers were likely a community of decapod crustaceans which built the structures to support dwelling/feeding activity (Curran, 1985; J. de Gibert, personal communication, 2012; Callow et al., 2013). All statistical measures of size distribution decrease above the K-Pg boundary (Table 1.1),

which indicates that the reduction in diameter is not an artifact of decreased variance (McShea, 1994; Smith et al., 2009). We attribute this size reduction as dwarfing within the post-extinction endobenthic community. Burrow diameters did not subsequently recover (increase) up section at any of the study localities in the measured stratigraphic intervals.

Figure 1.6 shows the proposed interpretation of endobenthic responses along the New Jersey coastal plain accompanying the mass extinction event. Within the Navesink/New Egypt Formations, the absence of burrows filled with Navesink/New Egypt sediment could be the result of minimal burrowing activity leading up to the extinction, or a function of poor trace-fossil preservation (Fig. 1.6A). Miller et al. (2010) suggested an increase in endobenthic activity along the New Jersey coastal plain following the extinction event. The ichnological evidence at Inversand, Rancocas, and Walnridge supports this hypothesis and may be analogous to shallow marine *Thalassinoides* occurring contemporaneous with spherule deposition in Spain (Rodríguez-Tovar et al., 2004; Rodríguez-Tovar, 2005).

The shift in burrow diameter occurs at the base of the MFL, which we interpret as the colonization surface from which most larger burrows originate (Fig. 1.6B). Since crustaceans are able to live in detritus-based trophic-food webs, it is likely that the community was able to thrive on the abundant organic matter associated with the extinction event (positive feedback of Morrow and Hasiotis, 2007). These burrows, which extended to nearly 2 m below the paleo-seafloor, were then filled with glauconite-rich sediment of the Hornerstown Formation as endobenthic colonization continued (Fig.

1.6C). After the abundant organic material from the K-Pg death assemblage was exhausted, possibly during the nutrient-deprived “Strangelove” oceanic period (Hsü and McKenzie, 1985; Kump, 1991), shrimp communities would have been stressed, which may account for the regional reduction in *Thalassinoides* burrow diameter (Urbanek, 1993; Smith et al., 2009; Morrow and Hasiotis, 2007). Strata representing this recovery period also contain the first appearance of actively filled (backfilled) meniscate burrows, which we interpret as evidence for a change in feeding strategy when detrital food sources became scarce (Buatois and Mángano, 2011).

The beige clay halo that outlines many burrows higher in the Hornerstown Formation may represent bioirrigation within the thalassinidean network. A detailed examination of the halo suggests that clay particles migrated through the larger glauconite grains of the burrow walls and were not actively emplaced by the tracemaker (Fig. 1.3E, F; Curran, 1985). Through recent laboratory experiments on shrimp burrows, Herringshaw and McIlroy (2012) have demonstrated that currents are produced both actively and passively to regulate fluid flow. These currents, which carry trace amounts of clay particles, can result in preferential accumulation of clays in sediments surrounding the burrow walls (Herringshaw and McIlroy, 2012). In deposits with higher clay content, such as the Navesink and New Egypt Formations, the lower permeability would not permit such diffusion to the same degree as in the Hornerstown Formation, which would explain the absence of the beige halo in the underlying units.

The trends in bioturbation across the K-Pg boundary can be interpreted as: (1) an increase in burrowing activity following the mass extinction, or (2) a gradual decrease in

sedimentation associated with reduced or constant burrowing activity. Previous work has demonstrated a gradual increase in glauconite maturity up-section at Inversand Quarry and Walnridge Farm, which is consistent with the latter interpretation (Obasi et al., 2011). The ichnological record also supports previous studies suggesting that the Hornerstown Formation was deposited in deeper water than the underlying Navesink/New Egypt sequences (Obasi et al., 2011 and references therein).

1.7 Conclusion

Abundant *Thalassinoides* burrows in marine K-Pg successions of New Jersey record a regional endobenthic response to the end-Cretaceous mass extinction (Fig. 1.6B; “positive feedback” of Morrow and Hasiotis, 2007). This is likely attributed to the ability of crustaceans to thrive on a detritus-based trophic-food web associated with the abundant organic matter generated by the extinction event (Schweitzer and Feldmann, 2005). As the organic detritus became scarce, tracemaker body size was substantially reduced (Lilliput effect of Urbanek, 1993; Fig. 1.5, 1.6C). An increase in ichnofabric index (Table 1.2), attributed to decreased sedimentation, is superimposed on what is likely a subsequent negative endobenthic feedback. As noted previously, endobenthic bioturbation may make it difficult to locate the K-Pg or other geologic boundaries by masking, moving, or diffusing diagnostic criteria. For example, the shocked quartz found in burrow fill below the MFL at Inversand (Obasi et al., 2011) may have been moved downward as sediment filled burrows. At Inversand, burrows more than one meter below the Navesink/Hornerstown contact are filled with Hornerstown sediments. Such sediment infills may also move Danian microfossils downward, possibly accounting for the

Table 1.1 – Results of the Kruskal-Wallis one-way ANOVA test evaluating burrow diameters from above (A) and below (B) the base of the MFL and/or iridium anomaly;

s = standard deviation; H = Chi-Square value corrected for ties; p = probability level.

	Inversand	Rancocas	Walnridge
	(n=345)	n=(284)	n=(201)
mean (A)	11.20	10.95	11.92
s (A)	3.59	3.07	3.19
	n=(536)	n=(294)	n=(107)
mean (B)	15.17	15.16	16.59
s (B)	4.79	5.00	4.72
H	143.27	117.79	68.30
p	<0.0001	<0.0001	<0.0001

Table 1.2 – Bioturbation index across the K-Pg boundary at Inversand, Rancocas, and Walnridge sites.

Position relative to basal Hornerstown Formation (cm)	Inversand	Rancocas	Walnridge
140	5	-	-
130	5	-	-
120	5	-	4
110	5	-	4
100	5	5	4
90	5	5	4
80	5	5	4
70	5	5	4
60	5	5	4
50	5	4	4
40	5	5	4
30	4	4	4
20	4	4	4
10	4	4	4
0	4	4	4
-10	3	3	4
-20	3	3	4
-30	4	3	3
-40	2	2	3
-50	2	2	4
-60	2	2	3
-70	2	3	3
-80	2	2	3
-90	2	3	3
-100	2	2	2
-110	2	-	2
-120	2	-	2
-130	2	-	2
-140	-	-	2
-150	-	-	2
-160	-	-	2

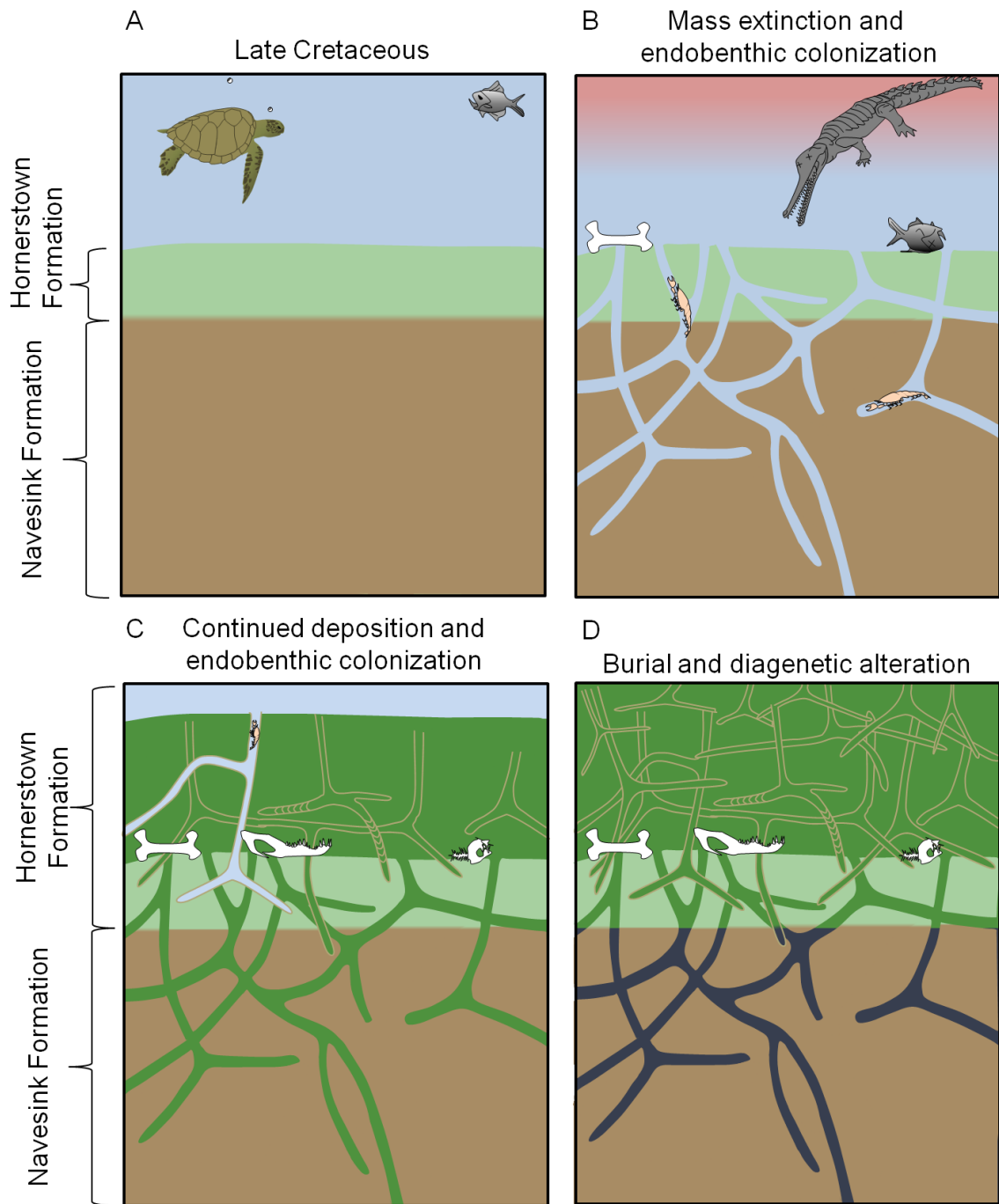


Figure 1.6 – Interpretive diagram of events surrounding the K-Pg mass extinction along the New Jersey coastal plain.

mixture of Cretaceous bones and Danian microfossils in the MFL (e.g., Self-Trail and Bybell, 1995). Bioturbation and diagenetic redox changes might also move or dilute Ir or other chemical anomalies (e.g., Colodner et al., 1992; Lee et al., 2003; Bigolsky et al., 2010; Ebel et al., 2010; Hull et al., 2011). Analysis of sediments for Ir or other trace element anomalies associated with meteorite impacts or ejecta is also more expensive and cannot be conducted in the field, and these anomalies may be diluted or moved by bioturbation or diagenesis. Because they are abundant, easy to measure, and are *in situ*, measurement of burrow diameters and morphology may allow much more rapid and certain placement of stratigraphic boundaries accompanying mass extinctions than the last or first occurrence of much less abundant vertebrate or even invertebrate macrofossils. This study demonstrates the potential applicability of paleoichnological analysis to other marine sections associated with major extinction events.

CHAPTER 2: ICHNOLOGICAL SIGNAL OF THE K-PG EVENT, BRAGGS, AL AND BRAZOS RIVER, TX

Manuscript in revision, Palaeogeography, Palaeoclimatology, Palaeoecology

(Wiest et al., accepted)

2.1 Abstract

As a proxy for the body size of the tracemaker, burrow diameter provides information on fundamental characteristics such as organism biology and behavior. Furthermore, changes in this endobenthic parameter provide insight into the timing and recovery of burrowing organisms in response to large-scale processes operating in ancient trophic systems. We herein report a decrease in burrow size in *Thalassinoides*-dominated ichnoassemblages across the Cretaceous-Paleogene (K-Pg) boundary in well studied shallow-marine sections along the Brazos River and Cottonmouth Creek, Texas and at Braggs, Alabama. At the Cottonmouth Creek and Brazos River localities, *Thalassinoides* isp. occurring above the previously reported negative $\delta^{13}\text{C}$ shift and the first occurrence of unequivocal Danian planktonic foraminifera are 17% smaller in short-axis diameter and 22% smaller when diameters are corrected for sediment compaction (mean K= 27.15 ± 7.12 mm, mean Pg= 21.13 ± 6.88 mm; n=53) than those excavated and filled prior to deposition of a hummocky cross-bedded, ejecta-bearing sandstone complex commonly interpreted as the Chicxulub ‘event deposit’. Across the K-Pg boundary at Braggs, diameters (D_{Th}) of simple maze *Thalassinoides* structures from similar, recurring depositional facies abruptly decrease by 22% (mean K= 13.08 ± 1.86 mm, mean Pg= 10.21 ± 1.87 mm; n=26). The Cretaceous and Paleogene burrows were preserved in

beds of similar lithology, suggesting the reduction in size is not attributed to sedimentological factors. At both localities, up-section trends in D_{Th} across the K-Pg boundary are statistically significant ($\alpha < 0.05$, non-parametric Kruskal-Wallis test) and reflect dwarfing within the post-extinction endobenthic community. These ichnological trends are similar to those recently documented at impact-distal sites along the New Jersey Coastal Plain. Dwarfing during the early recovery stages of the end-Cretaceous mass extinction, as recorded by trace fossils, was widespread and occurred within siliciclastic, carbonate, and glauconite-producing depositional environments. Since this ichnological signal in shallow marine successions appears to be a general phenomenon across the crisis interval, trace-fossil analysis provides a potential *in-situ* field method for constraining and correlating the stratigraphic position of the event, particularly in the absence of other macroscopic, microscopic, and geochemical indicators.

2.2 Introduction

Most major mass extinctions during the Phanerozoic resulted in a decrease in burrow diameter (Bottjer and Droser, 1994; Twitchett and Barras, 2004; Morrow and Hasiotis, 2007). As a proxy for tracemaker body size, burrow diameter provides information on fundamental characteristics such as organism biology and behavior (Twitchett and Barras, 2004; Morrow and Hasiotis, 2007). In continental environments, the Paleocene-Eocene Thermal Maximum is marked by a decrease in burrow diameter of soil fauna (Smith et al., 2009). Similarly, in marine settings, such as the Pilot Basin sequences of western Utah, the late Devonian extinction was marked by a reduction in

burrow size, as well as ichnodiversity and tier depth during the extinction, survival, and early recovery stages (Morrow and Hasiotis, 2007). A reduction in burrow size has also been documented at the Permian-Triassic boundary, which extended into the mid-Early Triassic (Twitchett and Wignall, 1996; Twitchett, 1999; Fraiser and Bottjer, 2000; Twitchett et al., 2001; Pruss and Bottjer, 2004; Twitchett and Barras, 2004; Twitchett et al. 2004; Pruss et al., 2005). The end-Triassic mass extinction was marked by a reduction in burrow size and tier depth as a response to potential widespread reduction in oxygen levels (Twitchett and Barras, 2004). Qualitative observations indicate ichnodiversity and burrow size are reduced at the Cretaceous-Paleogene (K-Pg) boundary in the lower Danian Fish Clay beds of Denmark (Ekdale and Bromley, 1984).

More recently, a significant decrease in *Thalassinoides* isp. burrow diameter (D_{Th}) was documented at the K-Pg boundary along the Atlantic Coastal Plain at several sites in New Jersey (Wiest et al., accepted). It remains unclear, however, if this reduction in burrow size is a regional signal to the large-scale environmental perturbation of the end-Cretaceous impact event, or part of a widespread response. In this paper we present new ichnological evidence for abrupt dwarfing from two Chicxulub impact-proximal sites along the Gulf Coastal Plain (Braggs, Alabama, and Brazos River, Texas; Fig 2.1), which indicates the widespread nature of the endobenthic response to the K-Pg event and thus serves as a potential stratigraphic correlation tool.

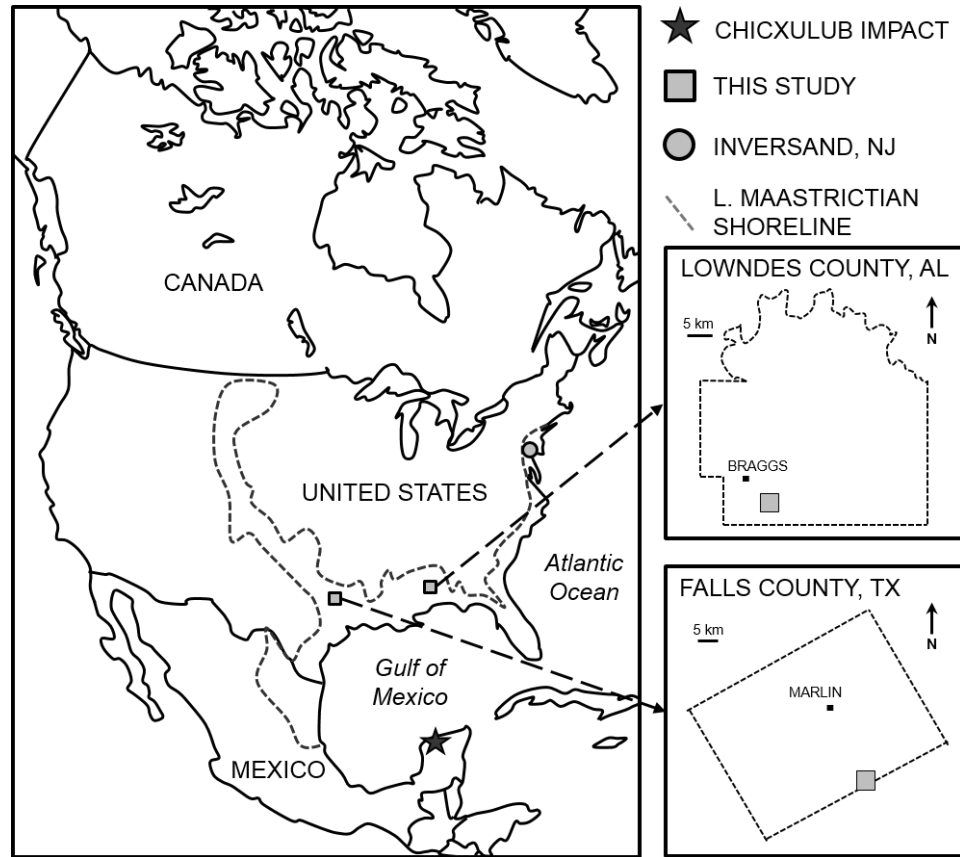


Figure 2.1 - Location map for studied K-Pg boundary sections. Squares = Brazos River (Texas) and Braggs (Alabama) sections; circle = Inversand Quarry, Sewell, NJ (Wiest et al., accepted). Position of the shoreline modified from Ron Blakey (www2.nau.edu).

2.3 Geologic Setting

2.3.1 Braggs, Alabama

The Upper Cretaceous (Maastrichtian) and Lower Paleogene (Danian) strata along State Highway 263 between Braggs and Greenville, Alabama (Fig. 2.1; 32° 0' 19" N, 86° 45' 1" W) consist of slightly southward-dipping, interbedded calcareous mudstone, sandstone and sandy limestone sequences which were deposited in a shallow marine environment (Copeland and Mancini, 1986; Jones et al., 1987; Donovan et al., 1988; Savrda, 1993). The exposed Upper Cretaceous sedimentary sequence is represented by the upper portion of the Prairie Bluff Formation and the lowermost 1 m of the Pine Barren Member of the Clayton Formation (Fig. 2.2). The formational contact is an erosional unconformity at the base of an indurated sandy limestone bed (Fig. 2.2, Bed 3; Copeland and Mancini, 1986). Jones et al. (1987), Donovan et al. (1988), Bryan and Jones (1989), and Zachos et al. (1989) placed the K-Pg boundary approximately 1 m above the formational contact, between beds 5 and 6 (Fig. 2.2). This boundary was established exclusively based on calcareous nanoplankton and occurs within a known magnetic reversal interval (Jones et al., 1987; Channell and Dobson, 1989). However, Habib et al. (1992) reported Danian nanoplankton in Bed 4 and placed the K-Pg boundary at the formational contact between beds 2 and 3. Likewise, Olsson and Liu (1993) assigned the period boundary to the top of the Prairie Bluff Chalk because Paleocene planktonic and benthic foraminiferal species were observed in bed 3, although rare and poorly preserved. Iridium peaks (≤ 0.7 ppb) have been reported within bed 2 and at the top of beds 5 and 9 (Donovan et al., 1988). Still, the K-Pg boundary section at

Braggs is likely incomplete because neither the negative shift in $\delta^{13}\text{C}$, nor the latest Maastrichtian/earliest Danian index foraminifera are present (Cepek et al., 1968; Gibson et al., 1982; Donovan et al., 1988; Zachos et al., 1989; Habib et al., 1992).

2.3.2 Brazos River and Cottonmouth Creek, Texas

The Cottonmouth Creek site, located on a tributary of the Brazos River just south of the FM-413 Bridge in Falls County, Texas (Fig. 2.1; 31° 6' 57" N, 96° 49' 57" W), contains exceptional exposures of the K-Pg succession (Keller et al., 2007; Keller, 2012; Hart et al. 2012). Units A1 and A3 (Fig. 2.3) are Latest Maastrichtian in age, dark gray, weakly-bedded claystone separated by a thin layer of yellow cheto smectite (A2), which Hart et al. (2012) interpreted as weathered volcanic ash. These units comprise the upper portion of the Corsicana Formation and were deposited in a low-oxygen, shallow marine environment (Keller et al., 2007). Overlying Unit A3, across an erosional unconformity, is a hummocky, cross-bedded sandstone (Unit HCS) with multiple fining upward sequences and abundant impact-derived spherules (Schulte et al., 2006; Keller et al., 2007; Abramovich et al., 2011; Adatte et al., 2011; Munsel et al., 2011). This unit is commonly referred to as the 'event deposit' by many workers and is interpreted as a single catastrophic tsunami deposit or a series of tempestites generated by the bolide impact (Bourgeois et al., 1988; Smit et al., 1996; Gale, 2006; Schulte et al., 2006; Hart et al., 2012). However, truncated trace fossils and multiple colonization surfaces within this "event deposit" complex in Texas and northeastern Mexico provide strong evidence which refutes this interpretation and suggest that deposition occurred over many years instead of hours or days (Stinnesbeck et al., 1993; Ekdale and Stinnesbeck, 1998).

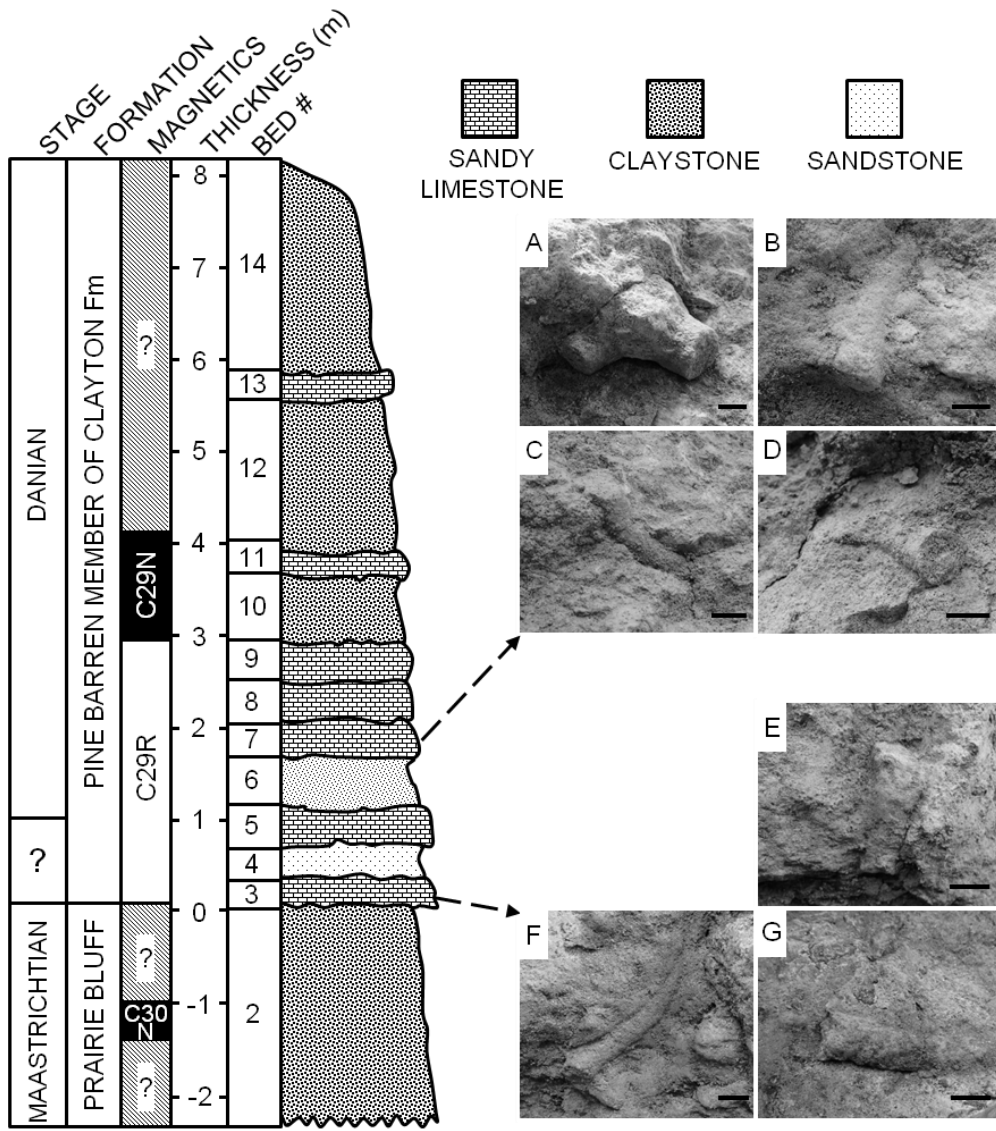


Figure 2.2 - Lithologic units and nomenclature of the Brags K-Pg boundary section modified from Copeland and Mancini (1986), and Jones et al. (1987). Position of K-Pg boundary after Donovan et al. (1988), Bryan and Jones (1989), and Zachos et al. (1989). Magnetic stratigraphy data from Channel and Dobson (1989). Insets A-D are images of burrows from Bed 7. Note the vertical Y-branch of inset A. Insets E-G are cross-section images of burrows from Bed 3. Scale bars; 1 cm.

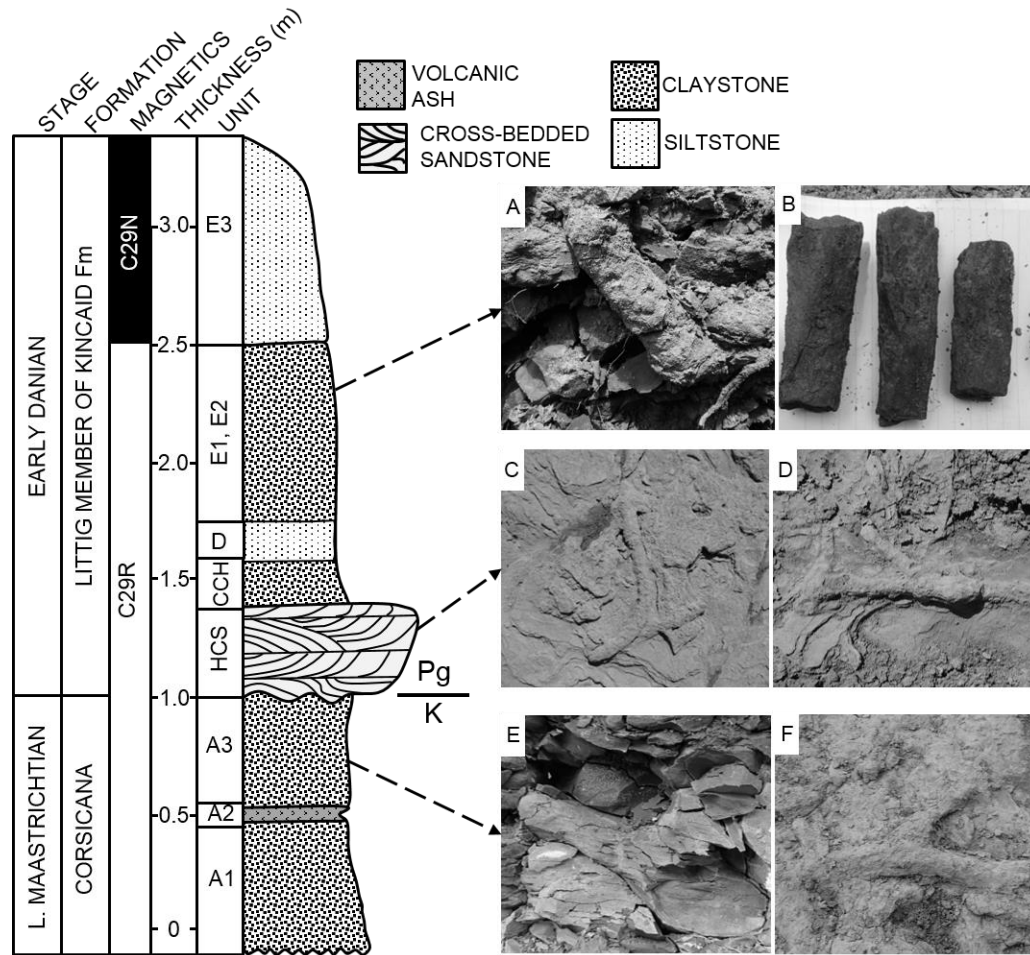


Figure 2.3 - Lithologic units and nomenclature of the Braggs K-Pg boundary section modified from Keller et al. (2007). Position of K-Pg boundary based on the International Commission on Stratigraphy (ICS) definition of the boundary as the base of the ejecta layer (Schulte et al., 2006 and Hart et al., 2012). Magnetic stratigraphy data from Keller et al. (2007). Insets A-B are images of burrows recovered from Unit E2, approximately 98 cm above the event deposit (HCS); Insets C-D are bedding-plane images of burrows recovered during this study from Unit HCS; Insets E-F are cross-section and bedding-plane images, respectively, of burrows recovered from Unit A3. Scale bars; 2 cm.

Above Unit HCS, the lithology returns to a gray, weakly-bedded claystone, similar to that of A1 and A3, which comprises the lower portion of the Littig Member of the Kincaid Formation (Keller et al., 2007). Approximately 2 km to the northeast, HCS and its bounding units are also exposed in bedding planes and cross-sections along the Brazos River (Munsel et al., 2011; 31° 7' 41" N, 96° 49' 19" W). In these sections, the K-Pg boundary coincides with the erosional surface between Units A3 and HSC based on the International Commission on Stratigraphy (ICS) definition of the boundary as the base of the ejecta layer (Cowie et al., 1989; Schulte et al., 2006). However, a discrepancy remains in the placement of the K-Pg boundary since the negative $\delta^{13}\text{C}$ shift and the first appearance of Danian planktonic foraminifera both occur ~ 80 cm above the event deposit (Keller et al., 2007; Abramovich et al., 2011; Keller, 2012).

2.4 Methods

At the Braggs, Brazos River, and Cottonmouth Creek localities (Fig. 2.1), a total of eleven fresh exposures were excavated and measured across the K-Pg boundary as designated by previous paleontological, geochemical, and sedimentological studies (Copeland and Mancini, 1986; Donovan and Vail, 1986; Zachos and Arthur, 1986; Jones et al., 1987; Donovan et al., 1988; Mancini et al., 1989; Olsson and Liu, 1993; Gale, 2006; Schulte et al., 2006; Keller et al., 2007; Abramovich et al., 2011; Adatte et al., 2011; Munsel et al., 2011). At each previously described section, all bioturbation structures were examined for surficial and architectural morphology, as well as fill characteristics. The ichnofabric index (ii) scale of Droser and Bottjer (1986) was assessed using the field method of Miller and Smail (1997). At each locality, only the units with

similar lithology containing well-defined, smooth-walled, branching traces (shafts and tunnels) characteristic of *Thalassinoides* isp. were chosen for study (Figs. 2.2 and 2.3). Inner diameters of shafts and tunnels (D_{Th}) were measured in the field and laboratory using digital vernier calipers to the nearest 0.01 mm. For burrows that were compacted, the original cross-section was reconstructed as an average of the short (vertical) and long (horizontal) axes. Measurements near enlarged junctions were avoided to ensure consistency. For each lithologic unit, the mean D_{Th} , standard deviation, and standard error were calculated. Median D_{Th} values below and above the K-Pg boundary and contained within similar rock types were compared using a non-parametric Kruskal-Wallis test (Davis, 1986; Smith et al., 2009).

2.5 Results & Discussion

2.5.1 Braggs, Alabama

The ichnofabric index of Beds 3 and 7 is ~ 2 and contains burrows of similar morphology (Fig. 2.2). The burrows are smooth walled, sub-vertical to horizontal, and exhibit occasional branching. These traces are characterized as simple mazes of *Thalassinoides* because box-work morphology was not observed. Burrows in these stratigraphic units are filled with material similar in grain size and lithology to the surrounding matrix, suggesting they originated from the same stratigraphic layer in which they were constructed. Burrows in Bed 3 range from ~ 9 to 16 mm in diameter with $D_{Th} = 13.08 \pm 1.86$ mm (n=15). Burrows in Bed 7 range from ~ 8 to 14 mm in diameter with $D_{Th} = 10.21 \pm 1.87$ mm (n=12; Appendix 4). Since burrows from these two units are of

the same ichnogenus and are contained within similar, recurring depositional facies, their mean D_{Th} were compared with a non-parametric Kruskal-Wallis test (Davis, 1986; Smith et al., 2009). Results of the analysis (Table 2.1) reveal that the diameters are significantly different ($H = 10.5$, $p < 0.001$, Table 2.1). Because the reduction in burrow diameter occurs between the top of bed 3 (stratigraphic origin of burrows from bed 3) and bed 7, we conclude that the environmental stress, as manifested by reduced body size within the survival community, occurred after deposition of bed 3. This suggests that either: 1) the reduction in body size was delayed, or 2) the Paleocene microfossils in bed 3 are the result of translocation into burrows from overlying strata. Recent work in the K-Pg boundary sequences of New Jersey tends to support the latter interpretation (Wiest et al., 2012b, accepted; Horner et al., 2013).

2.5.2 Brazos River & Cottonmouth Creek, Texas

The ichnofabric index of Unit A3 is approximately 3-4. Burrows recovered from A3 were smooth-walled, branching, and generally filled with dark gray claystone similar to the matrix, with rare sand-filled burrows. This indicates that almost the entire ichnoassemblage from A3 was established and filled prior to the deposition of the event deposit; however, the rare occurrence of sand-filled burrows suggests organisms within HCS were capable of penetrating the underlying erosional contact. The short-axis (vertical) diameter of *Thalassinoides* structures from A3 range from ~ 11 to 36 mm with a mean $D_{Th} = 21.55 \pm 5.65$ mm ($n=42$; Appendix 5). Similarly, Unit E2 contains a monospecific ichnoassemblage with ~ 8-27 mm size range (D_{Th} of 17.91 ± 5.83 mm;

n=11), and are filled with fine-grained material similar to the surrounding matrix. The ichnofabric index of the upper portion of Unit E2 is approximately 2-3.

The HCS event deposit is less bioturbated than underlying units (ii ~ 1-3) and contains *Thalassinoides*, *Ophiomorpha* and *Planolites* burrows (Smit et al., 1996; Gale, 2006; Keller et al., 2007). *Thalassinoides* burrows measured in this study (Fig. 2.3, C-D) were filled with sandy material similar to the surrounding matrix, which suggests they did not originate from the overlying claystone or siltstone units. These burrows range from ~ 6-26 mm in short-axis diameter with a mean D_{Th} of 12.52 ± 4.39 mm (n=93). Whereas *Thalassinoides* structures within the spherule-rich, cross-bedded sandstone complex may represent burrows constructed shortly after the impact event (e.g., Rodríguez-Tovar et al., 2004; Rodríguez-Tovar, 2005), the difference in mean D_{Th} within HCS, in comparison to mean D_{Th} from underlying and overlying units, cannot be singularly attributed to dwarfing as a result of environmental stresses; the distinct lithofacies shift, coupled with differences in grain size, may provide an alternative explanation for changes in burrow diameter.

Measured burrows from E2 were approximately 98 cm above the ‘event deposit’, which indicates they were constructed after the Chicxulub impact, negative $\delta^{13}C$ shift, and first occurrence of Danian planktonic foraminifera, so they represent structures of the post-extinction recovery interval. Also, burrows from E2 are similar in grain size and lithology to that of unit A3. These values were compared with a non-parametric Kruskal-Wallis test (Davis, 1986; Smith et al., 2009) and reveal a statistically significant difference across the K-Pg boundary.

Unlike the trace fossils from Inversand and Braggs, moderate compaction of burrows at Brazos River resulted in varying degrees of vertical shortening of the circular tunnels of Units A3, HCS and E2. The vertical- to horizontal-axis ratios of burrows from these units average 1.52, 1.48, and 1.36, respectively. When these ratios are used to correct for the compaction (average of vertical and horizontal axes), the short-axis diameter of burrows from A3 and HCS are increased more than those of E2, thus, the difference in burrow size across the K-Pg boundary is increased to 22% and remains significantly different ($H= 4.81$; $p=0.028$). For this reason, a 17% reduction in diameter represents a minimum decrease during the early Paleogene at the Brazos River locality. See Table 2.1 and Figure 2.4 for statistical information on burrow diameters and corrections for compaction. Field observations suggest that at ~3-4 m above the event deposit, *Thalassinoides* return to their pre-extinction size (Malcolm Hart, personal communication, 2013).

These findings suggest endobenthic organisms from siliciclastic (TX), carbonate (AL), and glauconite-dominated (NJ) depositional environments responded similarly to the environmental stresses in the aftermath of the end-Cretaceous extinction event. Thus, the endobenthic dwarfing phenomenon crossed at least these three mid-shelf depositional environments, irrespective of paleo-depth, and occurred along the Atlantic and Gulf Coastal Plains.

Table 2.1 - Results of the Kruskal-Wallis one-way ANOVA test evaluating burrow diameters from above (A) and below (B) the K-Pg boundary at Braggs, AL and Brazos, TX. Inversand data from Wiest et al., (accepted); s = standard deviation; H = Chi-Square value corrected for ties; p = probability level.

	Braggs, AL	Brazos, TX	Inversand, NJ
	(n=12)	(n=11)	(n=345)
mean (A)	10.21	21.13	11.20
s (A)	1.87	6.88	3.59
	(n=14)	(n=42)	(n=536)
mean (B)	13.08	27.15	15.17
s (B)	1.86	7.12	4.79
H	10.50	4.81	143.27
p	0.001	0.028	<0.001

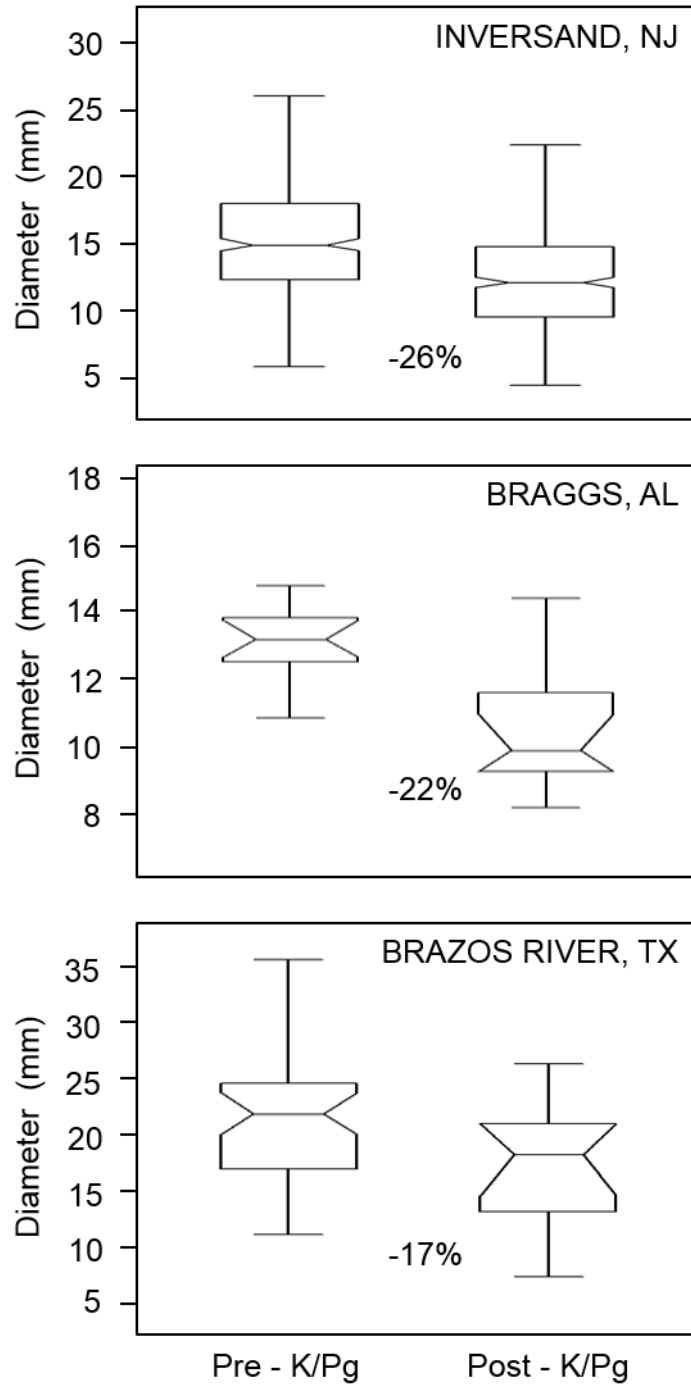


Figure 2.4 - Box and whisker plots of burrow diameters across the K-Pg boundary at the Braggs and Brazos localities. Inversand data from Wiest et al., (accepted). Note the differences in vertical scale.

2.6 Conclusions

The ichnological trends across the K-Pg boundary at the Brazos River and Braggs localities are interpreted as a strong response to the end-Cretaceous extinction event by infaunal decapod crustaceans. A similar reaction to this event was also documented in the glauconite-dominated K-Pg sequences along the New Jersey Coastal Plain, suggesting that dwarfing of the endobenthic community was a widespread response.

The survival of crustaceans in shallow marine environments following the end-Cretaceous mass extinction is likely attributed to their ability to burrow and scavenge (Sheehan and Hansen, 1986; Harries et al., 1996; Sheehan et al., 1996; Robertson et al., 2004, 2013; Schweitzer and Feldmann, 2005). However, the environmental stresses associated with the extinction event resulted in a decrease in body size within the endobenthic community, which manifested as a reduction of burrow diameter just above the K-Pg boundary. This dwarfism of infaunal organisms extended from the Atlantic Coastal Plain of New Jersey to the Gulf Coastal Plain with no apparent impact-proximal/distal trends (Table 2.1). As the ichnological signal in marine successions appears to be a widespread phenomenon across the crisis interval, trace-fossil analysis provides a potential field method for constraining and correlating the stratigraphic position of the event, particularly in the absence of other macroscopic, microscopic, and geochemical indicators.

CHAPTER 3: RECENT OVERPRINTING OF K-PG

***THALASSINOIDES* BY BURROWING INSECTS, SEWELL, NJ**

Manuscript in press, ICHNIA-2012 Proceedings, Geological Association of Canada

(Wiest and Buynevich, 2014)

3.1 Abstract

Cretaceous/Paleogene marine ichnofossils are overprinted by morphologically similar recent continental traces in unconsolidated successions at Inversand Quarry, Sewell, New Jersey. Within the glauconitic sand-dominated Hornerstown Formation, *Thalassinoides* burrow frameworks contain traces of burrowing bees and wasps. Because bee burrows may penetrate up to 1 m into the soft sediment, excavations just beyond the weathering front are not sufficient to remove modern overprinting. Insect burrow diameters (7-25 mm) are within the range of *Thalassinoides* traces (4-31 mm). Therefore neither size nor gross morphology are adequate for distinguishing these widely diachronous and unrelated ichnites, especially when the insect burrows have been filled. The presence of backfill menisci and a beige clay halo help distinguish the marine burrows, whereas highly oxidized fill and the presence of a terminal brooding chamber are diagnostic of modern insect burrows.

3.2 Introduction

Ichnocoenosis and ichnofabric analysis provide insight crucial to proper interpretation of ancient environments and erosional/depositional events. However,

careful consideration must be given when ecologically different and highly diachronous ichnoassemblages occur in unconsolidated sedimentary successions (Lockley and Hunt, 1995; Martin and Rindsberg, 2011; Donovan and Pawson, 2013). This is particularly true for traces with similar size and morphology, such as crustacean and insect burrows (Hasiotis and Bown, 1992).

The Inversand Company mine is a glauconite quarry in southern New Jersey that contains a productive bonebed and a heavily bioturbated Cretaceous-Paleogene (K-Pg) boundary section (Figs. 3.1 and 3.2). Previous studies have revealed an iridium excursion (Gallagher, 2012), as well as shocked quartz (Obasi et al., 2011), as evidence of the stratigraphic position of the boundary. However iridium and shocked quartz may have been subsequently reworked by endobenthic organisms. Despite the confounding influence of the traces on the depositional history, recent studies have demonstrated that ichnological analysis, due to its *in situ* context, can be effective for defining the stratigraphic relationships between the K-Pg boundary, lithologic contacts, and the fossiliferous layer (Wiest et al., 2012b, accepted). The ichnocoenosis has been described as a regionally extensive, monospecific assemblage of *Thalassinoides* isp. (*Th*), with an up-section increase in bioturbation (Wiest et al., 2012a). However, on many natural and excavated exposures, terrestrial insects have altered the original ichnofabric by overprinting the *Th* with traces of similar size and gross morphology. Here we document the geological context and physical characteristics of marine and continental ichnofossils at the Inversand locality. Our findings provide a framework for recognizing the

overprinting in the field in order to avoid confusion when reconstructing the depositional history of the K-Pg boundary sections along the Atlantic Coastal Plain.

3.3 Geologic Setting

The Inversand Mine at Sewell, New Jersey (39° 45'48" N, 75° 7'40" W) (Fig. 3.1) is a greensand extraction operation famous for its Late Cretaceous Main Fossiliferous Layer (MFL), as well as one of the best exposed K-Pg sections along the coastal plain. The Upper Cretaceous and Lower Paleogene formations consist of slightly southeastward-dipping, unconsolidated glauconite-rich sequences which were deposited in a mid-to-inner-shelf environment during several transgressive and regressive cycles (Gallagher, 1993; Bennington, 2003; Miller et al., 2004, 2010; Obasi et al., 2011). The lower Navesink Formation is a ~3-m-thick olive gray to dusky brown clayey-glauconitic sand (Minard et al., 1969; Owens et al., 1970) with *Th* ichnofabric indices ranging from 2 to 4. The overlying Hornerstown Formation is a 5.5-meter-thick fine-to-medium-grained glauconitic sand (Minard et al., 1969), with ichnofabric indices increasing up-section from 4 to 6 (Wiest et al., 2012a). The K-Pg boundary has been tentatively placed at 20 cm above the lithologic contact (Staron et al., 2001; Gallagher, 2012; Wiest et al., 2012b).

3.4 Methods

Fresh excavations at eight localities within the quarry were compared to outcrops exposed for varying amounts of time, ranging from several days to decades based on

phases of mining operations (Fig. 3.2A). Real-time visual observations and macro-photography were focused on insect activity adjacent to hollow burrows and related features (larvae, pupae) within brooding chambers. A number of representative active insect burrows were cast with Smooth-Cast 300Q resin. The inner diameters of *Th*, as well as insect traces (*in situ* and casts), were measured with a standard digital caliper. Burrows were examined for their surficial and architectural morphology, as well as fill characteristics and diagenetic effects.

3.5 Results

The Navesink Formation exhibits only a monospecific *Th* ichnoassemblage, regardless of duration of subaerial exposure. Burrows in this section were most easily recognized by their very dark bluish-gray color and nearly pure glauconite fill, contrasting with a dusky brown glauconitic-clay matrix. The vertical to sub-vertical shafts branch into a horizontal network of tunnels, which are unlined and do not display any backfill menisci.

Similarly, fresh exposures of >1 m into the lower 2 m of the Hornerstown Formation contain only the *Th* framework. The burrows exhibit both passive (Fig. 3.2B) and active (Fig. 3.2C) backfill, with beige clay halos. Bioturbation increases up section, with T, Y, and X-junctions revealed in all orientations, although branching is most common in the bedding-plane exposure.



Figure 3.1 – Location map of study site: Star indicates position of Inversand Quarry.

At many localities, the exposed portions of the Hornerstown Formation contain a second type of trace, which always cross-cuts or truncates the *Thalassinoides*. Occurring up to 1 m into the lateral section, these structures are generally sub-vertical (Fig. 3.3A) and branch occasionally (Fig. 3.3B). Typically, these are simple burrows ~10-60 cm in length with a slightly enlarged terminal chamber. Some of them are hollow and contain live pupae or abandoned cocoons within the chambers. Most of the overprinting structures contain oxidized glauconite sand and are more consolidated than the surrounding matrix, particularly in the outcrops that have been exposed for a prolonged period of time. When oxidized, the burrows and terminal chambers are accentuated by weathering (Fig. 3.4A,B). During the spring and summer months, digger bees (*Andrena* sp., Fig. 3.4A, inset) were observed in association with the simple structures. Digger wasps (*Sphex* sp., Fig. 3.4B, inset), although rare, were documented in proximity with the hollow, branching burrows. The diameters of the hollow and oxidized insect burrows range between 7 and 25 mm (n=20), and fall within the dimensions of *Thalassinoides* which range between 4 and 29 mm (n=883; Wiest et al., 2012a) at this site (Fig. 3.5). These simple structures are absent in the Navesink Formation.

3.6 Discussion

The *Thalassinoides* burrow network in the exposed K-Pg succession of southern New Jersey is overprinted by modern digging insects. The insect burrows can be attributed to the observed digger bees and wasps and is also confirmed by the presence of live pupae within terminal brooding chambers (Hasiotis, 2002). However, for much of the year, the tracemakers cannot be observed within the quarry. Bee and wasp burrows

can be distinguished by means of casting and careful analysis of the terminal brooding chamber. The chambers of a digger bee burrow are more smooth, symmetrical, and regular than that of the wasp (Evans, 1966; S. Hasiotis, personal communication, 2012). The absence of insect traces in the Navesink Formation suggests that the digger bees and wasps tend to favor a sandy, less consolidated substrate over a firmer substrate with higher clay content (Ghazoul, 2001). Also, waterlogging of the Navesink Formation makes it less habitable for these insects (Rodríguez-Tovar, 2007).

Since modern insects can penetrate the ancient substrate deeper and more rapidly than the influence of modern weathering, trenching to remove the veneer of modern soil formation may not be sufficient to clearly observe the unaltered ichnofabric. Because decapod crustaceans are the *Thalassinoides* tracemaker, the size, branching, and orientation of fossil burrow segments are comparable to the passively filled modern insect traces (Seilacher, 2007, Plates 16 & 17; J. De Gibert, personal communication, 2012). In this case, gross burrow morphology and fill are not adequate for distinguishing between the continental and marine traces. However, the presence of backfill menisci and a beige clay halo (possibly indicative of bioirrigation; Herringshaw and McIlroy, 2012) can be used as an indicator of thalassinidean origin. In contrast, a highly oxidized fill and the presence of a terminal brooding chamber are diagnostic of modern insect burrows (Hasiotis, 2002).

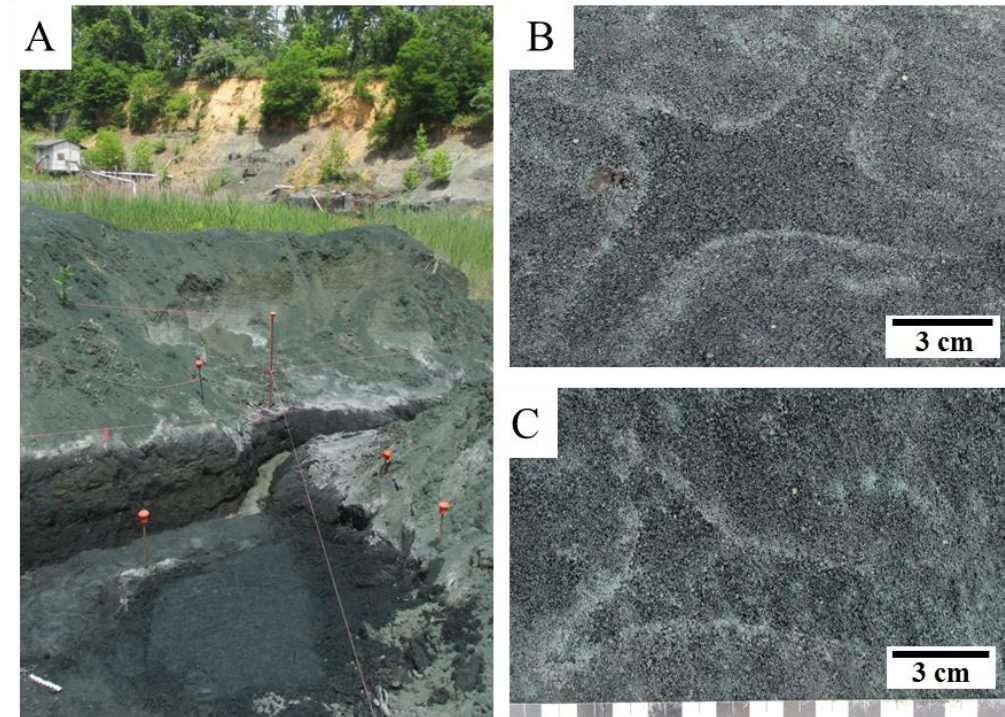


Figure 3.2 – A) Photograph of the Inversand quarry. In the foreground, the horizontal plane has been freshly excavated, whereas the outcrop in the trench wall has been exposed for several months and has few insect traces. The embankment in the background has been exposed for several decades and has numerous insect burrows. B) Bedding-plane view of a freshly exposed *Thalassinoides* isp. exhibiting an X-junction. C) An actively filled *Thalassinoides* Y-junction and menisci.

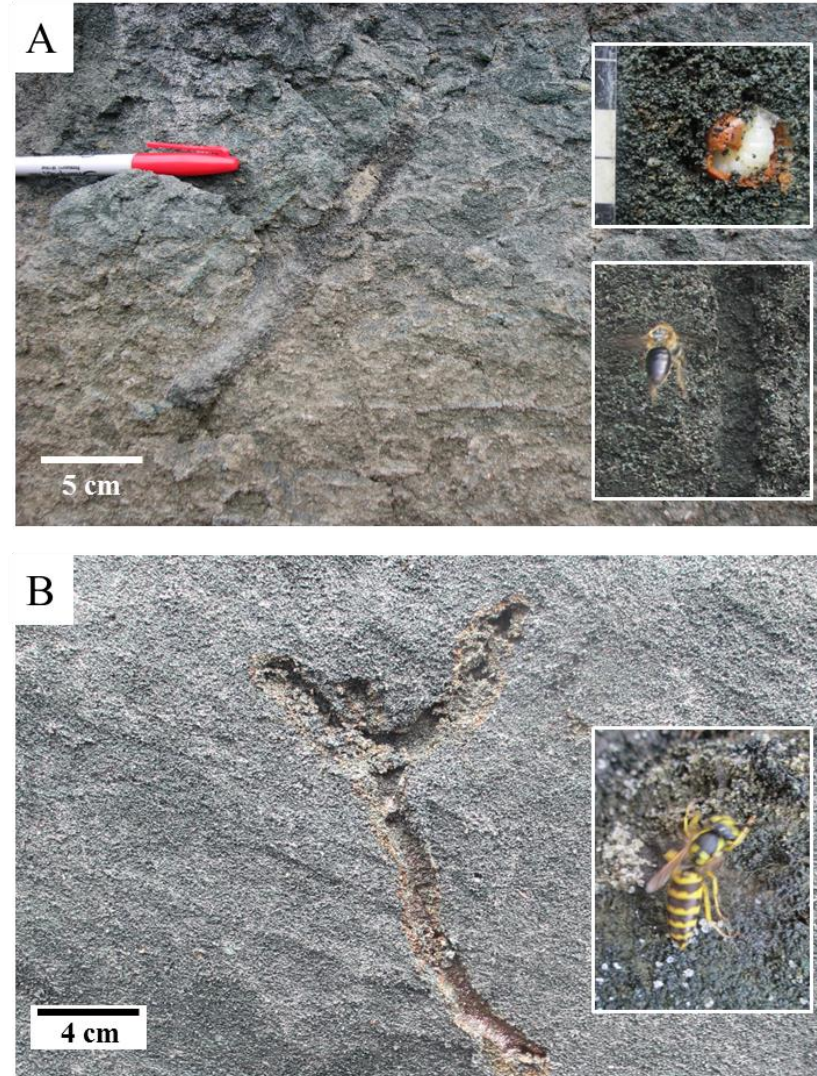


Figure 3.3 – A) A sub-vertical, infilled insect trace cross-cutting a network of *Thalassinoides* of similar size. Inset in upper right is a live pupa and cocoon found within a hollow insect burrow. Inset in lower right shows a digger bee (~10 mm long) found in association with unbranching hollow burrows. B) Cross-sectional view of a branching, vertical insect trace in a completely bioturbated portion of the Hornerstown Formation. Inset is of a wasp (~12 mm long) observed adjacent to the more complex insect traces.

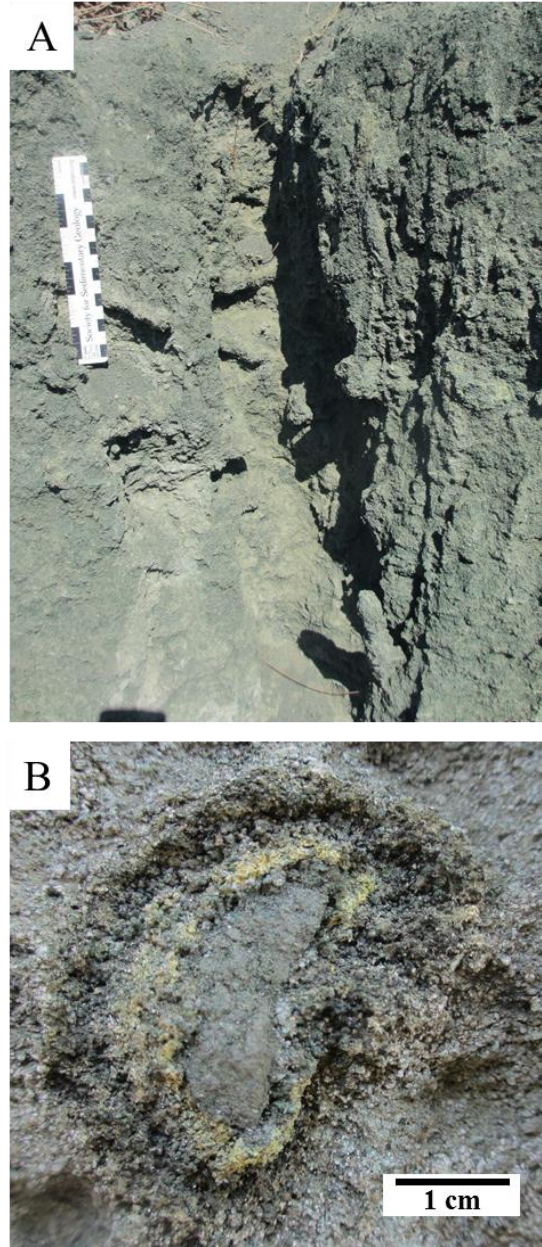


Figure 3.4 – A) Naturally weathered surface containing both ancient marine and modern continental ichnofossils. Note that oxidized insect traces are more resistant to weathering, whereas the original fossil ichnoassemblage has the same weathering properties as the surrounding matrix. B) Cross-sectional view of a modern oxidized terminal chamber exposed by erosion.

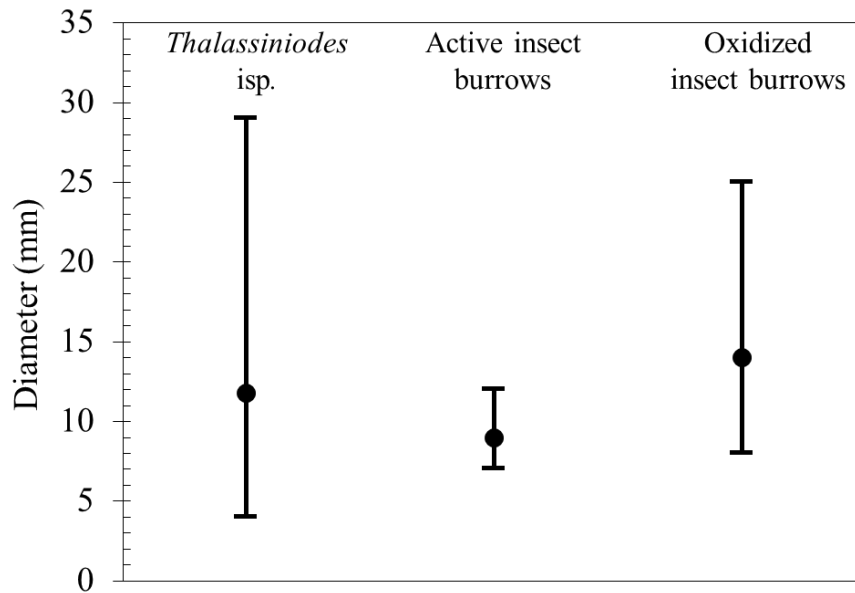


Figure 3.5 – Mean, minimum, and maximum burrow diameters of *Th*, active insect burrows, and oxidized insect burrows from the Hornerstown Formation. Size overlap indicates that insect burrows cannot be distinguished from the marine traces based on size, particularly in the case of smaller *Th* burrows.

3.7 Conclusions

When studying semi-lithified marine successions, overprinting by continental biotic communities must be considered (Martin and Rindsberg, 2011). Within the glauconitic sand-dominated Paleogene Hornerstown Formation of southern New Jersey, *Th* burrow frameworks are occasionally penetrated by modern digger bees and wasps. Due to their lateral extent and penetration depth of up to 1 m, excavations just beyond the weathering front are insufficient for exposing the original marine ichnofabric. Despite the similarities between infilled marine and continental ichnofossils, several diagnostic criteria aid in distinguishing them in outcrops.

REFERENCES

- Abramovich, S., Keller, G., Berner, Z., Cymbalista, M., and Rak, C., 2011, Maastrichtian Planktic Foraminiferal Biostratigraphy and Paleoenvironment of Brazos River, Falls County, Texas, U.S.A.: SEPM, Special Publication No. 100, p. 123-156.
- Adatte, T., Keller, G., and Baum, G., 2011, Age and Origin of the Chicxulub Impact and Sandstone Complex, Brazos River, Texas: Evidence from Lithostratigraphy and Sedimentology: SEPM, Special Publication No. 100, p. 43-80.
- Baird, D., 1967, Age of fossil birds from the greensands of New Jersey: *The Auk*, v. 84, p. 260–262.
- Bennington, J.B., 2003, Paleontology and sequence stratigraphy of the Upper Cretaceous Navesink Formation, New Jersey: Long Island geologists field trip, 18 October 2003, Hofstra University.
- Bigolski, J.N., Ebel, D.S., Landman, N.H., Boesenberg, J.S., and Hsieh, C-T., 2010, Ni and Co in pyrite framboids from Agony Creek section, K/Pg boundary in the New Jersey coastal plain: *Geological Society of America Abstracts with Programs*, v. 42, p. 305.
- Bottjer, D.J. and Droser, M.L., 1994, The history of Phanerozoic bioturbation, *in* Donovan, S.K. ed., *The Paleobiology of Trace Fossils*: John Hopkins, Baltimore, p. 155–176.
- Bourgeois, J., Hansen, T.A., Wiberg, P., and Kauffman, E.G., 1988, A tsunami deposit at the Cretaceous–Tertiary boundary in Texas: *Science*, v. 141, p. 567–570.

- Bryan, J.R. and Jones, D.S., 1989, Fabric of the Cretaceous–Tertiary marine macrofaunal transition at Braggs, Alabama: *Palaeogeography, Palaeoclimatology, Palaeoecology*, v. 69, p. 279–30.
- Buatois, L. and Mángano, M.G., 2011, *Ichnology: Organism-Substrate Interactions in Space and Time*: Cambridge University Press, 358 p.
- Callow, R.H.T., McIlroy, D., Kneller, B., and Dykstra, M., 2013, Ichnology of Late Cretaceous Turbidites from the Rosario Formation, Baja California, Mexico: *Ichnos*, v. 20, p. 1-14.
- Cepek, P., Hay, W.W., Masters, B.A., and Worsley, T.R., 1968, Calcareous plankton in samples from field trip stops, in Scott, J.C., chairman, *Facies changes in the Selma Group in central and eastern Alabama*: University, Alabama, Alabama Geological Society Sixth Annual Fieldtrip Guidebook, p. 33-40.
- Channell, J.E.T. and Dobson, J.P., 1989, Magnetic stratigraphy and magnetic mineralogy at the Cretaceous-Tertiary boundary section, Braggs, Alabama: *Palaeogeography, Palaeoclimatology, Palaeoecology*, v. 69, p. 267-277.
- Colodner, D.C., Boyle, E.A., Edmond, J.M., and Thomson, J., 1992, Postdepositional mobility of platinum, iridium and rhenium in marine-sediments: *Nature*, v. 358, p. 402-404.
- Copeland, C.W. and Mancini, E.A., 1986, Cretaceous Tertiary boundary southeast of Braggs, Lowndes County, Alabama, *in* T.L. Neathery ed., *Southeastern Section of the Geological Society of America: Centennial Field Guide*, v. 6, p. 369-372.

- Cowie, J.W., Zieger, W., and Remane, J., 1989, Stratigraphic Commission accelerates progress, 1984-1989: *Episodes*, v. 112, p. 79-83.
- Curran, H.A., 1985, The trace fossil assemblage of a Cretaceous nearshore environment: Englishtown formation of Delaware, USA: *SEPM Special Publications*, v. 35, 261-76.
- Davis, J.C., 1986, *Statistics and Data Analysis in Geology*, 2nd Edition: John Wiley & Sons, New York, 646 p.
- Donovan, A. D., Baum, G. R., Blechschmidt, G. L., Loutit, T. S., Pflum, C. E., and Vail, P. R., 1988, Sequence stratigraphic setting of the Cretaceous-Tertiary boundary in central Alabama, in: Wilgus, C. K., ed., *Sea Level Changes - An Intergrated Approach*: *SEPM, Spec. Publ.*, p. 42.
- Donovan, A. D. and Vail, P. R., 1986, Sequence stratigraphy of the K-T boundary in Alabama: 10 Yaxcopoil-1 drilling site, Chicxulub impact structure: Petrography, geochemistry, and depositional environment: *Meteoritics & Planetary Science*, v. 39, p. 857–878.
- Donovan, S.K. and Pawson, D.J., 2013, An intersection in time and space: Significance of modern invertebrate borings in Upper Cretaceous Echinoids: *Ichnos*, v. 20, p.81-87.
- Droser, M.L. and Bottjer, D.J., 1986, A semiquantitative field classification of ichnofabric: *Journal of Sedimentary Petrology*, v. 56, p. 558–559.

- Ebel, D.S., Hsieh, C-T., Landman, N.H., and Boesenberg, J.S., 2010, Ni and Co in pyrite mark the K/Pg boundary in Crosswicks Creek section, New Jersey coastal plain. Geological Society of America Abstracts with Programs, v. 42, p. 305.
- Ekdale, A.A. and Bromley, R.G., 1984, Sedimentology and ichnology of the Cretaceous-Tertiary boundary in Denmark: implications for the causes of the terminal Cretaceous extinction: *Journal of Sedimentary Petrology*, v. 54, p. 681–703.
- Ekdale, A.A. and Stinnesbeck, W., 1998, Trace fossils in Cretaceous–Tertiary (KT) boundary beds in northeastern Mexico: implications for sedimentation during the KT boundary event: *PALAIOS*, v. 13, p. 593–602.
- Evans, H.E., 1966, *The comparative ethology and evolution of the sand wasps*: Harvard Univ. Press, Cambridge, 540 p..
- Fraiser, M.L., and Bottjer, D.J., 2000, The U-shaped trace fossil *Arenicolites*: burrow of an opportunist during the biotic recovery from the end-Permian mass extinction: Geological Society of America Abstracts with Programs, 32(7), 368.
- Gale, A.S., 2006, The Cretaceous–Palaeogene boundary on the Brazos River, Falls County, Texas: Is there evidence for impact-induced tsunami sedimentation?: *Proceedings of the Geologists' Association*, v. 117, p. 173–185.
- Gallagher, W.B., 1984, Paleoecology of the Delaware Valley region, Part II: Cretaceous to Quaternary: *The Mosasaur*, v. 2, p. 9–43.
- Gallagher, W.B., 1990, Biostratigraphy and paleoecology of the Upper Cretaceous–Lower Tertiary sequence in the New Jersey Coastal Plain: Ph.D. Dissertation, University of Pennsylvania, Philadelphia, 402 p.

- Gallagher, W.B., 1993, The Cretaceous Tertiary extinction event in the northern Atlantic coastal plain: *The Mosasaur*, v. 5, p. 75–154.
- Gallagher, W.B., 2002, Faunal changes across the Cretaceous Tertiary (K–T) boundary in the Atlantic coastal plain of New Jersey: restructuring the marine community after the K–T mass-extinction event, *in* Koeberl, C., and MacLeod, K.G., eds., *Catastrophic Events and Mass Extinctions: Impacts and Beyond*: Geological Society of America, Special Paper 356, p. 291–301.
- Gallagher, W.B., 2003, Oligotrophic oceans and minimalist organisms: collapse of the Maastrichtian marine ecosystem and Paleocene recovery in the Cretaceous-Tertiary sequence of New Jersey, *in* Schulp, A.S. and Jagt, J.W.M., eds., *Proceedings of the First Mosasaur Meeting*: *Netherlands Journal of Geosciences*, v. 82, p. 225-231.
- Gallagher, W.B., 2012, Comparative taphonomy of Late Cretaceous vertebrate fossil occurrences in the Atlantic Coastal Plain deposits of Appalachia: testing the hypothesis of mass mortality at the K-Pg boundary: *Journal of Vertebrate Paleontology*, Program and Abstracts, p. 18.
- Gallagher, W.B., Parris, D.C., and Spamer, E.E., 1986, Paleontology, biostratigraphy, and depositional environments of the Cretaceous–Tertiary transition in the New Jersey coastal plain: *The Mosasaur*, v. 3, p. 1–35.
- Gallagher, W.B., Parris, D.C., Grandstaff, B.S., Camburn, J. and Camburn, S., 2003, Comparative taphonomy of vertebrate fossil concentrations in the Late Cretaceous

– Early Tertiary sequence of New Jersey: *Journal of Vertebrate Paleontology* 23 (Suppl. to 3): 53A.

Gallagher, W.B., Miller, K.G., Shelrrell, R.M., Browning, J.V., Field, M.P., Olsson, R., Sugarman, P.J., Tuorto, S. and Wahyudi, H., 2012, On the last mosasaurs: Late Maastrichtian mosasaurs and the Cretaceous-Paleogene boundary in New Jersey. *Bulletin de la Societe Geologique de France*, v. 183, no. 2, p. 145-150.

Ghazoul, J., 2001, Effect of soil hardness on aggression in the solitary wasp *Mellinus arvensis*: *Ecological Entomology*, v. 26, p. 457–466.

Gibson, T.G., Mancini, E.A., and Bybell, L.M., 1982, Paleocene to middle Eocene stratigraphy of Alabama: *Gulf Coast Association of Geological Societies Transactions*, v. 32, p. 449-458.

Habib, D., Moshkovitz, S., and Kramer, C., 1992, Dinoflagellate change and calcareous nannofossil response to sea-level in Cretaceous-Tertiary boundary sections: *Geology*, v. 20, p. 165-168.

Harries, P.J., Kauffman, E.G., and Hansen, T.A., 1996, Models for biotic survival following mass extinction, *in* Hart, M.B. ed., *Biotic Recovery from Mass Extinction Events: The Geological Society, London, Special Publication 102*, p. 41–60.

Hart, M. B., Leighton, A. D., Yancey, T. E., Hampton, M., Miller, B. V., Liu, C., Smart, C. W., and Twitchett, R. J., 2012, Re-writing the Cretaceous-Paleogene boundary events in Texas: new sections and revised micropaleontological interpretations. *Geological Society of America Abstracts with Programs*. v. 44, 7, p. 325.

- Hasiotis, S.T., 2002, Continental Trace Fossils: SEPM, Short Course Notes No. 51, Tulsa, Oklahoma, 132 p.
- Hasiotis, S.T., and Bown, T.M., 1992, Invertebrate trace fossils: The backbone of continental Ichnology, *in* Maples, C.G., and West, R.R., eds., Trace Fossils: Short Courses in Paleontology no. 5, Paleontological Society.
- Herringshaw, L., and McIlroy, D., 2012, The fossil record of bioirrigation: ICHNIA 2012, St. John's, Newfoundland, Canada, p. 43.
- Horner, R.J., Wiest, L.A., Buynevich, I.V., Terry, D.O., Jr., and Grandstaff, D.E., 2013, Shrimp-trace elements: geochemistry of *Thalassinoides*-dominated marine K/Pg sections of New Jersey: Geological Society of America Abstracts with Programs, v. 45, n. 7.
- Hope, S., 1999, A new species of Graculavus from the Cretaceous of Wyoming, *in* Olson, S.L., ed., Smithsonian Contributions to Paleobiology: Smithsonian Institution, no. 89, p. 261–266.
- Hsü, K.J., and McKenzie, J.A., 1985, A “Strangelove” ocean in the earliest Tertiary, *in* Sundquist, E.T., and Broecker, W.S., eds., The Carbon Cycle and Atmospheric CO₂: Natural Variations Archean to Present: American Geophysical Union, Geophysical Monograph 32, p. 487–492.
- Hull, P.M., Franks, P.J.S., and Norris, R.D., 2011, Mechanisms and models of iridium anomaly shape across the Cretaceous-Paleogene boundary: Earth and Planetary Science Letters, v. 301, p. 98-106.

- Jones, D.S., Mueller, P.A., Bryan, J.R., Dobson, J.P., Channel, J. E. T., Zachos, J. C., and Arthur, M. A., 1987, Biotic, geochemical and paleomagnetic changes across the Cretaceous/Tertiary boundary at Braggs, Alabama: *Geology*, v. 15, p. 311-315.
- Keller, G., 2012, The Cretaceous-Tertiary Mass Extinction, Chicxulub Impact, and Deccan Volcanism: *Earth and Life*, International Year of Planet Earth, p. 759-793.
- Keller, G., Adatte, T., Berner, Z., Harting, M., Baum, G., Prauss, M., Tantawy, A., and Stuben, D., 2007, Chicxulub impact predates K–T boundary: New evidence from Brazos, Texas: *Earth and Planetary Science Letters*, v. 255, p. 339-356.
- Kennedy, W.J., and Cobban, W.A., 1996, Maastrichtian ammonites from the Hornerstown Formation in New Jersey: *Journal of Paleontology*, v. 70, p. 798–804.
- Koch, R.C., and Olsson, R.K., 1977, Dinoflagellate and planktonic foraminiferal biostratigraphy of the uppermost Cretaceous of New Jersey: *Journal of Paleontology*, v. 51, p. 480–491.
- Kump, L.R., 1991, Interpreting carbon-isotope excursions: Strangelove oceans: *Geology*, v. 19, p. 299-302.
- Landman, N.H., Johnson, R.O., and Edwards, L.E., 2004. Cephalopods from the Cretaceous/Tertiary boundary interval on the Atlantic coastal plain, with a description of the highest ammonite zones in North America. Part II. Northeastern Monmouth County, New Jersey: New York, American Museum of Natural History Bulletin 287, 107 p.

- Landman, N.H., Johnson, R.O., Garb, M.P., Edwards, L.E., and Kyte, F.T., 2007, Cephalopods from the Cretaceous/ Tertiary boundary interval on the Atlantic Coastal Plain, with a description of the highest ammonite zones in North America. Part III. Manasquan River basin, Monmouth County, New Jersey: New York, American Museum of Natural History Bulletin 303, 122 p.
- Lee, C-T.A., Wasserburg, G.J., and Kyte, F.T., 2003, Platinum-group elements (PGE) and rhenium in marine sediments across the Cretaceous-Tertiary boundary: constraints on Re-PGE transport in the marine environment: *Geochimica et Cosmochimica Acta*, v. 67, p. 655-670.
- Lockley, M.G. and Hunt, A.P., 1995, Dinosaur tracks and other fossil footprints of the western United States: Columbia University Press, 338 p.
- Mancini, E.A., Tew, B.H., and Smith, C.C., 1989, Cretaceous-Tertiary contact, Mississippi and Alabama: *Journal of Foraminiferal Research*, v. 19, p. 93-104.
- Martin, A.J. and Rindsberg, A.K., 2011, Ichnological diagnosis of ancient storm-washover fans, Yellow Banks Bluff, St. Catherines Island, *in* Bishop, G.A, Rollin, H.B., and Thomas, D.H., eds., *Geoarchaeology of St. Catherines Island, Georgia: Anthropological Papers of the American Museum of Natural History*, v. 94, p. 114-127.
- McShea, D.W., 1994, Mechanisms of large-scale evolutionary trends: *Evolution*, v. 48, p. 1747–1763.
- Miller, K.G., Sugarman, P.J., Browning, J.V., Kominz, M.A., Olsson, R.K., Feigenson, M.D., and Hernandez, J.C., 2004, Upper Cretaceous sequences and sea-level

- history, New Jersey coastal plain: Geological Society of America Bulletin, v. 116, p. 368–393, doi: 10.1130/B25279.1.
- Miller, K.G., Sherrell, R.M., Browning, J.V., Field, M.P., Gallagher, W.B., Olsson, R.K., Sugarman, P.J., Tuorto, S., and Wahyudi, H., 2010, Relationship between mass extinction and iridium across the Cretaceous–Paleogene boundary in New Jersey: *Geology*, v. 38, p. 867–870, doi: 10.1130/G31135.1.
- Miller, M.F., and Smail, S.E., 1997, A semiquantitative field method for evaluating bioturbation on bedding planes: *PALAIOS*, v. 12, p. 391-396.
- Minard, J.P., Owens, J.P., Sohl, N.F., Gill, H.E., and Mello, J.F., 1969, Cretaceous–Tertiary boundary in New Jersey, Delaware, and eastern Maryland: U.S. Geological Survey Bulletin 1274-H.
- Minard, J.P., Owens, J.P., and Sohl, N.F., 1976, Coastal Plain Stratigraphy of the Upper Chesapeake Bay Region: Geological Society of America, 61 p.
- Morrow, J.R., and Hasiotis, S.T., 2007, Infaunal response through mass-extinction episodes: predictive models and observed patterns, *in* Miller, W. III, ed., *Trace Fossils—Concepts, Problems, Prospects*: Elsevier Press, p. 575-598.
- Munsel, D., Berner, Z., and Stüben, D., 2011, The Sandstone Complex in the Brazos Riverbed Section: Geochemical Constraints on Genesis and Depositional Conditions: *SEPM, Special Publication No. 100*, p. 281-295.
- Obasi, C.C., Terry, D.O., Jr., Myer, G.H., and Grandstaff, D.E., 2011, Glauconite composition and morphology, shocked quartz, and the origin of the Cretaceous(?)

- Main Fossiliferous Layer (MFL) in southern New Jersey, U.S.A.: *Journal of Sedimentary Research*, v. 81, p. 479-494, doi: 10.2110/jsr.2011.42.
- Olsson, R.K., 1963, Latest Cretaceous and Early Tertiary stratigraphy of New Jersey coastal plain: *American Association Petroleum Geologists, Bulletin*, v. 47, p. 643–665.
- Olsson, R.K., Liu, C., 1993, Controversies on the placement of Cretaceous-Paleogene boundary and the K/P mass extinction of planktonic foraminifera. *PALAIOS*, v. 8, p. 127-139.
- Olsson, R.K., Miller, K.G., Browning, J.V., Hibab, D., and Sugarman, P.J., 1997, Ejecta layer at the Cretaceous–Tertiary boundary, Bass River, New Jersey (Ocean Drilling Program Leg 174AX): *Geology*, v. 25, p. 759–762.
- Olsson, R.K., Miller, K.G., Browning, J.V., Wright, J.D., and Cramer, B.S., 2002, Sequence stratigraphy and sea level change across the Cretaceous–Tertiary boundary on the New Jersey passive margin, *in* Koeberl, C., and MacLeod, K.G., eds., *Catastrophic Events and Mass Extinctions: Impacts and Beyond: Geological Society of America, Special Paper 356*, p. 97–108.
- Owens, J.P., Minard, J.P., Sohl, N.F., and Mello, J.F., 1970, Stratigraphy of the post-Magothy Upper Cretaceous formations in southern New Jersey and northern Delmarva Peninsula, Delaware and Maryland: U.S. Geological Survey Professional Paper 674, 60 p.
- Parris, D.C., 1974, Additional records of plesiosaurs from the Cretaceous of New Jersey: *Journal of Paleontology*, v. 48, p. 32–35.

- Pruss, S.B., and Bottjer, D.J., 2004, Early Triassic trace fossils of the western United States and their implications for prolonged environmental stress from the end-Permian mass extinction: *PALAIOS*, v. 19, p. 551–564.
- Pruss, S.B., Corsetti, F.A., and Bottjer, D.J., 2005, Environmental trends of Early Triassic biofabrics: implications for understanding the aftermath of the end-Permian mass extinction, *in* Over, D.J., Morrow, J.R., and Wignall, P.B., eds., *Understanding Late Devonian and Permian–Triassic Biotic and Climatic Events: Towards an Integrated Approach: Developments in Palaeontology and Stratigraphy*, Elsevier Pub., Amsterdam, v. 20, p. 313–332.
- Robertson, D.S., Lewis, W. M., Sheehan, P.M., and Toon, O.B., 2013, K-Pg extinction in marine and freshwater environments: The impact winter model: *Journal of Geophysical Research: Biogeosciences*, v. 118, p. 1-9.
- Robertson, D.S., McKenna, M.C., Toon, O.B., Hope, S. and Lillegraven, J.A., 2004, Survival in the first hours of the Cenozoic: *Geological Society of America Bulletin*, v. 116(5-6), p. 760–768.
- Rodríguez-Tovar, F.J., 2005, Fe-oxide spherules infilling *Thalassinoides* burrows at the Cretaceous–Paleogene (K–P) boundary; evidence of near-contemporaneous macrobenthic colonization during the K–P event: *Geology*, v. 33, p. 585–588.
- Rodríguez-Tovar, F.J., 2007, Substrate firmness controlling nesting behavior of *Bembix oculata* (Hymenoptera, Bembicinae), *in* Bromley R.G., Buatois, L.A., Mángano, M.G., Genise, J.F., Melchor, R.N., eds., *Sediment-organism interactions: a multifaceted ichnology*: *SEPM Special publication*, v. 88, p. 353–359.

- Rodríguez -Tovar, F.J., Martínez-Ruiz, F., and Bernasconi, S.M., 2004, Carbon isotope evidence for the timing of the Cretaceous-Palaeogene macrobenthic colonisation at the Agost section (southeast Spain): *Palaeogeography, Palaeoclimatology, Palaeoecology*, v. 203, p. 65–72, doi: 10.1016/S0031-0182(03)00660-6.
- Savrda, C.E., 1993, Ichnosedimentologic evidence for a noncatastrophic origin of Cretaceous-Tertiary boundary sands in Alabama: *Geology*, v. 21, p. 1075–1078, doi: 10.1130/0091-7613(1993)0212.3.CO;2.
- Schulte, P., Speijer, R., Mai, H., and Kontny, A., 2006, The Cretaceous–Paleogene (K–P) boundary at Brazos, Texas: Sequence stratigraphy, depositional events and the Chicxulub impact: *Sedimentary Geology*, v. 184, p. 77–109.
- Schweitzer, C.E. and Feldmann, R.M., 2005, Decapod crustaceans, the K/P event, and Palaeocene recovery, *in* Koenemann, S., and Jenner, R.A., eds., *Crustacea and arthropod relationships: Crustacean Issues*, v. 16, p. 17-53.
- Seilacher, A., 2007, *Trace Fossil Analysis*: Springer-Verlag Berlin Heidelberg, Berlin, p. 226.
- Self-Trail, J.M., and Bybell, L.M., 1995, Cretaceous and Paleogene calcareous nannofossil biostratigraphy of New Jersey, *in* Baker, J.E.B., ed., *Contributions to the Paleontology of New Jersey, Proceedings of a Symposium, Field Trips and Teacher Workshop on the Topic*: William Paterson College of New Jersey, Department of Environmental Science and Geography, Wayne, New Jersey, Annual Field Conference, Geological Association of New Jersey, v. 12, p. 102–139.

- Sheehan, P.M., Coorough, P.J., and Fastovsky, D.E., 1996, Biotic selectivity during the K/T and Late Ordovician extinction events, *in* Ryder, G., Fastovsky, D.E., and Gartner, S., eds., *The Cretaceous-Tertiary Event and Other Catastrophes in Earth History: Geological Society of America, Special Paper 307*, p. 183–195.
- Sheehan, P. M. and Hansen, T. A., 1986, Detrital feeding as a buffer to extinction at the end of the Cretaceous: *Geology*, v. 14, p. 868–870.
- Smit, J., Roep, T.B., Alvarez, W., Montanari, A., Claeys, P., Grajales-Nishimura, J.M., and Bermudez, J., 1996, Coarse-grained, clastic sandstone complex at the K/T boundary around the Gulf of Mexico: Deposition by tsunami waves induced by the Chicxulub impact?, *in* Ryder, G., Fastovsky, D.E., and Gartner, S., eds., *The Cretaceous–Tertiary Event and Other Catastrophes in Earth History: Geological Society of America, Special Paper 307*, p. 151–182.
- Smith, J.J., Hasiotis, S.T., Woody, D.T., and Kraus, M.J., 2009, Transient dwarfism of soil fauna during the Paleocene-Eocene Thermal Maximum: *Proceedings of the National Academy of Science, Early Edition*, p. 1–6, doi: 10.1073/pnas.0909674106.
- Staron, R.M., Grandstaff, B.S., Gallagher, W.B., and Grandstaff, D.E., 2001, REE signatures in vertebrate fossils from Sewell, New Jersey: implication for location of the K/T boundary: *PALAIOS*, v. 16, p. 255–265.
- Stinnesbeck, W., Barbarin, J.M., Keller, G., Lopez-Oliva, J.G., Pivnik, D.A., Lyons, J.B., Officer, C.B., Adatte, T., Graup, G., Rocchia, R., and Robin, E., 1993, Deposition of channel deposits near the Cretaceous–Tertiary boundary in northeastern

- Mexico: catastrophic or 'normal' sedimentary deposits?: *Geology*, v. 21, p. 797–800.
- Twitchett, R.J., 1999, Palaeoenvironments and faunal recovery after the end-Permian mass extinction: *Palaeogeography, Palaeoclimatology, Palaeoecology*, v. 154, p. 27–37.
- Twitchett, R.J., and Barras, C.G., 2004, Ichnostratigraphy and mass extinctions, *in* McIlroy, D., ed., *The Application of Ichnology to Palaeoenvironmental and Stratigraphic Analysis*: The Geological Society, London, Special Publication 228, p. 397–418.
- Twitchett, R.J., and Wignall, P.B., 1996, Trace fossils and the aftermath of the Permian-Triassic mass extinction; evidence from northern Italy: *Palaeogeography, Palaeoclimatology, Palaeoecology*, v. 124(1-2), p. 137–151.
- Twitchett, R.J., Looy, C.V., Morante, R., Visscher, H., and Wignall, P.B., 2001, Rapid and synchronous collapse of marine and terrestrial ecosystems during the end-Permian biotic crisis: *Geology*, v. 29, p. 351–354.
- Twitchett, R.J., Krystyn, L., Baud, A., Wheelley, J.R., and Richoz, S., 2004, Rapid marine recovery after the end-Permian mass-extinction event in the absence of marine anoxia: *Geology*, v. 32, p. 805–808.
- Urbanek, A., 1993, Biotic crises in the history of Upper Silurian graptoloids: a palaeobiological model: *Historical Biology*, v. 7, p. 29–50.
- Van Valen, L., 1994, The origin of plesiadapid primates and the nature of *Purgatorius*: *Evolutionary Monographs*, v. 15, p. 1-79.

- Wiest, L.A., and Buynevich, I.V., Recent overprinting of Cretaceous-Paleogene Thalassinoides framework by burrowing insects: ICHNIA-2012 Conference Volume, Geological Association of Canada, St. John's, Canada, in review.
- Wiest, L.A., Buynevich, I.V., Grandstaff, D.E., Terry, D.O., Jr., Maza, Z.A., Trace fossil evidence suggests widespread dwarfism in response to the end-Cretaceous mass extinction: Bragg, Alabama and Brazos River, Texas: *Palaeogeography, Palaeoclimatology, Palaeoecology*, in review.
- Wiest, L.A., Buynevich, I.V., Grandstaff, D.E., Terry, D.O., Jr., Lacovara, K.J. Ichnological evidence for endobenthic response and dwarfing at the K-Pg boundary, New Jersey, U.S.A.: *PALAIOS*, accepted.
- Wiest, L.A., Buynevich, I.V., Grandstaff, D.E., and Terry, D.O. Jr., 2012a, Ichnological evidence for dwarfism in endobenthic communities at the K-Pg interval in New Jersey, U.S.A.: paleoenvironmental disturbance and stratigraphic implications: ICHNIA 2012, St. John's, Newfoundland, Canada, p. 97.
- Wiest, L.A., Grandstaff, D.E., Terry, D.O. Jr., Lacovara, K.J., and Buynevich, I.V., 2012b, Ichnological constraints on the origin of the Main Fossiliferous Layer, New Jersey: *Geological Society of America Abstracts with Programs*, v. 44, p. 529.
- Wolfe, P.E., 1977, *The Geology and Landscapes of New Jersey*: New York, Crane, Russak, 351 p.
- Wroblewski, A.E.-J., 2008, Paleoenvironmental significance of Cretaceous and Paleocene *Psilonichnus* in southern Wyoming: *PALAIOS*, v. 23, p. 370-379.

Zachos, J. C. and Arthur, M. A., 1986, Paleooceanography of the Cretaceous/Tertiary boundary event: Inferences from stable isotopic and other data:

Paleooceanography, v. 1, p. 5-26.

Zachos, J. C., Arthur, M.A., and Dean, W.E., 1989, Geochemical and paleoenvironmental variations across the Cretaceous/Tertiary boundary at Braggs, Alabama:

Palaeogeography, Palaeoclimatology, Palaeoecology, v, 69, p. 245-266.

APPENDIX A: D_{7h} AND STRATIGRAPHIC POSITION AT INVERSAND

Sample Number	Depth relative to basal MFL (cm)	Burrow Diameter (mm)
I- 1	131	10.58
I- 2	130	8.89
I- 3	130	5.83
I- 4	129	10.78
I- 5	129	10.75
I- 6	129	11.45
I- 7	128	14.96
I- 8	128	9.72
I- 9	128	14.42
I- 10	128	11.20
I- 11	127	10.63
I- 12	127	8.02
I- 13	127	10.19
I- 14	127	10.91
I- 15	127	16.16
I- 16	126	6.94
I- 17	126	8.07
I- 18	125	11.61
I- 19	125	6.28
I- 20	125	11.94
I- 21	124	6.33
I- 22	123	12.85
I- 23	123	7.50
I- 24	123	12.38
I- 25	123	12.78
I- 26	123	13.09
I- 27	122	5.31
I- 28	122	4.82
I- 29	122	12.93
I- 30	122	9.91
I- 31	122	4.63
I- 32	121	6.90
I- 33	120	8.94
I- 34	120	10.46

APPENDIX A (CONTINUED): D_{Th} AND POSITION AT INVERSAND

Sample Number	Depth relative to basal MFL (cm)	Diameter (mm)
I- 35	120	11.13
I- 36	120	9.11
I- 37	119	14.27
I- 38	119	15.01
I- 39	119	8.00
I- 40	119	4.01
I- 41	118	13.03
I- 42	118	16.63
I- 43	117	7.21
I- 44	116	10.69
I- 45	115	13.59
I- 46	115	14.81
I- 47	114	4.91
I- 48	113	12.38
I- 49	113	11.26
I- 50	112	10.24
I- 51	112	4.58
I- 52	112	10.12
I- 53	111	16.90
I- 54	111	16.60
I- 55	111	11.66
I- 56	110	6.39
I- 57	109	12.18
I- 58	109	11.02
I- 59	108	11.17
I- 60	108	6.02
I- 61	107	13.64
I- 62	107	11.96
I- 63	107	14.59
I- 64	107	11.66
I- 65	105	11.40
I- 66	105	14.86
I- 67	104	10.13
I- 68	103	13.67
I- 69	103	5.66

APPENDIX A (CONTINUED): D_{Th} AND POSITION AT INVERSAND

Sample Number	Depth relative to basal MFL (cm)	Diameter (mm)
I- 70	103	11.09
I- 73	102	12.54
I- 74	102	4.24
I- 75	102	11.03
I- 76	102	13.92
I- 77	101	14.82
I- 78	101	12.16
I- 79	101	9.11
I- 80	101	12.18
I- 81	101	4.31
I- 82	100	7.75
I- 83	100	9.37
I- 84	100	14.46
I- 85	100	9.62
I- 86	100	14.81
I- 87	99	15.03
I- 88	99	15.45
I- 89	99	14.77
I- 90	99	11.01
I- 91	99	9.95
I- 92	98	12.01
I- 93	98	10.98
I- 94	98	12.64
I- 95	98	8.75
I- 96	97	13.28
I- 97	97	8.22
I- 98	97	5.40
I- 99	95	13.75
I- 100	95	8.04
I- 101	94	4.49
I- 102	94	19.88
I- 103	94	11.25
I- 104	94	15.14
I- 105	93	8.79
I- 106	93	11.58

APPENDIX A (CONTINUED): D_{Th} AND POSITION AT INVERSAND

Sample Number	Depth relative to basal MFL (cm)	Diameter (mm)
I- 107	93	14.48
I- 108	93	7.85
I- 109	93	15.72
I- 110	93	12.31
I- 111	92	10.19
I- 112	91	12.55
I- 113	91	7.38
I- 114	90	14.66
I- 115	89	13.16
I- 116	89	8.10
I- 117	89	17.96
I- 118	89	5.18
I- 119	88	8.01
I- 120	88	20.16
I- 121	88	14.08
I- 122	88	10.53
I- 123	88	8.68
I- 124	87	10.36
I- 125	87	6.00
I- 126	87	13.88
I- 127	87	14.36
I- 128	86	8.04
I- 129	86	16.21
I- 130	86	12.70
I- 131	86	11.33
I- 132	86	10.20
I- 133	85	7.49
I- 134	85	16.07
I- 135	84	15.62
I- 136	84	11.05
I- 137	84	13.10
I- 138	84	11.28
I- 139	83	14.35
I- 140	83	12.88
I- 141	83	9.77

APPENDIX A (CONTINUED): D_{Th} AND POSITION AT INVERSAND

Sample Number	Depth relative to basal MFL (cm)	Diameter (mm)
I- 142	82	13.54
I- 143	82	13.84
I- 144	82	10.61
I- 145	82	4.31
I- 146	81	13.55
I- 147	81	7.42
I- 148	81	12.73
I- 149	81	8.43
I- 150	80	9.32
I- 151	80	9.03
I- 152	79	17.73
I- 153	79	12.47
I- 154	79	10.22
I- 155	79	9.56
I- 156	78	14.50
I- 157	78	14.86
I- 158	78	3.59
I- 159	78	18.51
I- 160	78	6.76
I- 161	78	9.25
I- 162	78	15.87
I- 163	78	4.96
I- 164	77	12.05
I- 165	77	9.03
I- 166	77	8.95
I- 167	76	14.10
I- 168	76	9.86
I- 169	76	9.68
I- 170	76	12.15
I- 171	75	11.38
I- 172	75	8.74
I- 173	75	10.14
I- 174	75	6.48
I- 175	75	13.18
I- 176	75	8.11

APPENDIX A (CONTINUED): D_{Th} AND POSITION AT INVERSAND

Sample Number	Depth relative to basal MFL (cm)	Diameter (mm)
I- 177	75	4.86
I- 178	74	12.89
I- 179	74	6.81
I- 180	74	14.04
I- 181	73	6.93
I- 182	73	12.61
I- 183	73	6.62
I- 184	72	13.08
I- 185	72	11.38
I- 186	72	13.38
I- 187	72	8.77
I- 188	72	10.01
I- 189	72	7.94
I- 190	71	11.56
I- 191	71	12.99
I- 192	70	9.07
I- 193	70	9.32
I- 194	70	12.47
I- 195	70	9.94
I- 196	70	22.15
I- 197	70	9.53
I- 198	69	18.31
I- 199	69	11.92
I- 200	69	9.59
I- 201	69	8.85
I- 202	69	5.82
I- 203	68	11.20
I- 204	68	9.31
I- 205	68	6.64
I- 206	68	13.72
I- 207	68	8.06
I- 208	67	9.83
I- 209	67	14.01
I- 210	66	5.73
I- 211	66	10.82

APPENDIX A (CONTINUED): D_{Th} AND POSITION AT INVERSAND

Sample Number	Depth relative to basal MFL (cm)	Diameter (mm)
I- 212	66	10.93
I- 213	66	5.15
I- 214	65	22.51
I- 215	65	14.64
I- 216	65	4.58
I- 217	64	8.49
I- 218	62	11.93
I- 219	61	6.12
I- 220	61	11.66
I- 221	61	8.38
I- 222	60	11.68
I- 223	60	12.37
I- 224	60	10.85
I- 225	60	14.02
I- 226	60	19.21
I- 227	60	13.11
I- 228	59	12.40
I- 229	59	6.27
I- 230	59	6.27
I- 231	59	15.11
I- 232	59	5.94
I- 233	59	7.57
I- 234	59	8.97
I- 235	59	9.27
I- 236	59	10.21
I- 237	58	10.41
I- 238	58	12.88
I- 239	58	13.06
I- 240	58	13.08
I- 241	58	13.74
I- 242	58	15.65
I- 243	58	4.73
I- 244	56	13.64
I- 245	56	15.56
I- 246	56	8.65

APPENDIX A (CONTINUED): D_{Th} AND POSITION AT INVERSAND

Sample Number	Depth relative to basal MFL (cm)	Diameter (mm)
I- 247	55	14.07
I- 248	55	12.63
I- 249	55	12.96
I- 250	54	11.54
I- 251	53	9.15
I- 253	52	11.87
I- 254	51	11.74
I- 255	51	10.74
I- 256	51	12.34
I- 257	51	14.59
I- 258	50	11.56
I- 259	50	15.63
I- 260	50	9.93
I- 261	50	10.30
I- 262	50	8.63
I- 263	50	5.23
I- 264	49	15.37
I- 265	49	3.54
I- 266	49	10.76
I- 267	49	16.31
I- 268	48	15.80
I- 269	48	6.38
I- 270	48	9.25
I- 271	48	14.48
I- 272	48	4.94
I- 273	46	9.07
I- 274	45	14.50
I- 275	44	16.36
I- 276	42	10.96
I- 277	42	17.43
I- 278	41	10.97
I- 279	41	8.73
I- 280	41	10.38
I- 281	40	4.23
I- 282	40	13.00

APPENDIX A (CONTINUED): D_{Th} AND POSITION AT INVERSAND

Sample Number	Depth relative to basal MFL (cm)	Diameter (mm)
I- 283	40	9.19
I- 284	39	9.91
I- 285	38	16.14
I- 286	37	17.73
I- 287	37	6.98
I- 288	37	5.37
I- 289	36	15.62
I- 290	36	14.18
I- 291	35	11.03
I- 292	35	16.63
I- 293	34	16.94
I- 294	33	14.35
I- 295	33	11.73
I- 296	32	16.48
I- 297	32	11.15
I- 298	32	8.99
I- 299	32	13.03
I- 300	32	8.00
I- 301	32	8.08
I- 302	32	14.15
I- 303	32	6.45
I- 304	32	17.02
I- 305	31	12.22
I- 306	31	10.40
I- 307	31	6.88
I- 308	30	8.48
I- 309	30	12.40
I- 310	30	17.53
I- 311	30	8.03
I- 312	30	15.14
I- 313	30	16.67
I- 314	29	13.67
I- 315	29	10.13
I- 316	29	8.00
I- 317	29	7.57

APPENDIX A (CONTINUED): D_{Th} AND POSITION AT INVERSAND

Sample Number	Depth relative to basal MFL (cm)	Diameter (mm)
I- 318	29	10.88
I- 319	28	17.53
I- 320	28	10.16
I- 321	27	17.55
I- 322	27	15.35
I- 323	27	8.37
I- 324	26	7.87
I- 325	26	18.72
I- 326	26	9.53
I- 327	26	17.15
I- 328	25	12.12
I- 329	25	16.56
I- 330	25	14.42
I- 331	24	9.96
I- 332	24	8.89
I- 333	24	15.93
I- 334	24	11.71
I- 335	23	5.89
I- 336	23	14.71
I- 337	23	13.18
I- 338	22	16.41
I- 339	22	10.41
I- 340	22	12.12
I- 341	22	4.22
I- 342	21	9.55
I- 343	21	13.89
I- 344	21	13.63
I- 345	21	12.06
I- 346	20	13.61
I- 347	20	9.78
I- 348	20	10.69
I- 349	20	15.29
I- 350	20	10.51
I- 351	20	14.77
I- 352	20	13.30

APPENDIX A (CONTINUED): D_{Th} AND POSITION AT INVERSAND

Sample Number	Depth relative to basal MFL (cm)	Diameter (mm)
I- 353	19	14.78
I- 354	19	15.57
I- 355	19	14.55
I- 356	19	11.89
I- 357	19	8.13
I- 358	19	11.00
I- 359	19	14.96
I- 360	19	19.86
I- 361	19	10.31
I- 362	19	6.76
I- 363	19	10.17
I- 364	19	21.83
I- 365	19	10.63
I- 366	19	11.31
I- 367	18	18.42
I- 368	18	12.65
I- 369	18	20.02
I- 370	18	10.97
I- 371	18	17.48
I- 372	18	12.07
I- 373	18	24.05
I- 374	18	16.59
I- 375	18	20.13
I- 376	18	15.83
I- 377	18	14.88
I- 378	17	22.00
I- 379	17	20.40
I- 380	17	15.27
I- 381	17	18.75
I- 382	17	22.96
I- 383	17	12.32
I- 384	17	5.29
I- 385	17	18.28
I- 386	17	10.93

APPENDIX A (CONTINUED): D_{Th} AND POSITION AT INVERSAND

Sample Number	Depth relative to basal MFL (cm)	Diameter (mm)
I- 387	16	17.27
I- 388	16	16.00
I- 389	16	11.96
I- 390	16	10.21
I- 391	16	25.07
I- 392	16	8.26
I- 393	16	14.38
I- 394	16	22.38
I- 395	16	10.86
I- 396	16	7.70
I- 397	16	13.70
I- 398	15	13.36
I- 399	15	9.75
I- 400	15	15.14
I- 401	15	6.55
I- 402	15	25.45
I- 403	15	10.50
I- 404	14	21.92
I- 405	14	20.93
I- 406	14	11.24
I- 407	14	12.17
I- 408	13	19.02
I- 409	13	16.33
I- 410	13	13.06
I- 411	12	16.26
I- 412	12	8.13
I- 413	12	23.90
I- 414	12	15.32
I- 415	12	8.99
I- 416	12	6.62
I- 417	11	12.55
I- 418	10	23.09
I- 419	10	20.04
I- 420	10	16.33
I- 421	10	24.74

APPENDIX A (CONTINUED): D_{Th} AND POSITION AT INVERSAND

Sample Number	Depth relative to basal MFL (cm)	Diameter (mm)
I- 422	10	10.74
I- 423	10	6.96
I- 424	10	14.73
I- 425	10	5.03
I- 426	10	13.11
I- 427	10	15.52
I- 428	10	25.81
I- 429	9	16.97
I- 430	9	10.41
I- 431	9	17.96
I- 432	9	12.67
I- 433	9	15.28
I- 434	9	14.96
I- 435	8	24.43
I- 436	8	14.63
I- 437	8	20.02
I- 438	8	19.61
I- 439	8	24.10
I- 440	8	12.57
I- 441	8	17.23
I- 442	8	12.46
I- 443	8	8.91
I- 444	8	13.22
I- 445	8	17.91
I- 446	8	11.94
I- 447	7	21.62
I- 448	7	18.77
I- 449	7	13.72
I- 450	7	10.52
I- 451	7	9.30
I- 452	7	8.76
I- 453	7	11.79
I- 454	7	10.87
I- 455	6	20.78
I- 456	6	15.85

APPENDIX A (CONTINUED): D_{Th} AND POSITION AT INVERSAND

Sample Number	Depth relative to basal MFL (cm)	Diameter (mm)
I- 457	6	20.17
I- 458	6	16.32
I- 459	6	17.89
I- 460	5	7.87
I- 461	5	20.28
I- 462	5	6.09
I- 463	5	9.35
I- 464	5	16.08
I- 465	4	21.74
I- 466	4	11.94
I- 467	4	8.81
I- 468	4	5.99
I- 469	4	19.41
I- 470	4	12.42
I- 471	4	20.26
I- 472	4	8.09
I- 473	4	13.99
I- 474	4	18.84
I- 475	4	15.55
I- 476	4	6.00
I- 477	4	8.12
I- 478	4	25.82
I- 479	3	17.22
I- 480	3	5.63
I- 481	3	9.92
I- 482	3	15.71
I- 483	3	12.56
I- 484	3	12.88
I- 485	3	16.38
I- 486	3	20.76
I- 487	3	18.04
I- 488	2	14.07
I- 489	2	9.60
I- 490	2	7.44
I- 491	2	21.26

APPENDIX A (CONTINUED): D_{Th} AND POSITION AT INVERSAND

Sample Number	Depth relative to basal MFL (cm)	Diameter (mm)
I- 492	1	10.67
I- 493	1	8.66
I- 494	1	19.52
I- 495	1	8.79
I- 496	1	17.93
I- 497	1	12.75
I- 498	1	8.86
I- 499	1	27.62
I- 500	1	16.58
I- 501	1	14.65
I- 502	1	14.42
I- 503	0	8.48
I- 504	0	25.53
I- 505	0	13.32
I- 506	0	22.87
I- 507	0	9.96
I- 508	-1	14.55
I- 509	-1	12.75
I- 510	-1	11.49
I- 511	-1	14.91
I- 512	-1	10.08
I- 513	-1	11.49
I- 514	-2	19.51
I- 515	-2	18.54
I- 516	-2	17.50
I- 517	-2	20.15
I- 518	-2	9.84
I- 519	-2	15.03
I- 520	-2	16.86
I- 521	-2	21.74
I- 522	-3	16.54
I- 523	-3	17.65
I- 524	-3	21.02
I- 525	-4	13.49
I- 526	-4	23.98

APPENDIX A (CONTINUED): D_{Th} AND POSITION AT INVERSAND

Sample Number	Depth relative to basal MFL (cm)	Diameter (mm)
I- 527	-4	19.30
I- 528	-4	14.35
I- 529	-4	12.13
I- 530	-4	22.00
I- 531	-5	21.69
I- 532	-5	30.15
I- 533	-5	15.49
I- 534	-5	12.96
I- 535	-5	17.16
I- 536	-6	20.40
I- 537	-6	11.25
I- 538	-6	8.92
I- 539	-6	20.89
I- 540	-6	7.40
I- 541	-6	18.31
I- 542	-7	7.92
I- 543	-7	20.02
I- 544	-7	13.58
I- 545	-8	17.93
I- 546	-8	12.41
I- 547	-8	7.03
I- 548	-8	22.65
I- 549	-8	19.55
I- 550	-9	20.57
I- 551	-9	14.55
I- 552	-9	15.85
I- 553	-9	22.97
I- 554	-9	11.83
I- 555	-9	9.15
I- 556	-9	16.93
I- 557	-9	12.54
I- 558	-10	20.68
I- 559	-10	19.43
I- 560	-10	13.56
I- 561	-10	9.40

APPENDIX A (CONTINUED): D_{Th} AND POSITION AT INVERSAND

Sample Number	Depth relative to basal MFL (cm)	Diameter (mm)
I- 562	-10	18.34
I- 563	-10	26.49
I- 564	-10	27.08
I- 565	-10	10.55
I- 566	-10	20.65
I- 567	-10	24.74
I- 568	-11	22.07
I- 569	-11	12.50
I- 570	-11	16.48
I- 571	-11	11.80
I- 572	-11	16.94
I- 573	-11	12.74
I- 574	-12	17.42
I- 575	-12	10.16
I- 576	-12	21.67
I- 577	-12	9.39
I- 578	-12	11.58
I- 579	-13	17.86
I- 580	-13	16.51
I- 581	-13	13.93
I- 582	-13	15.21
I- 583	-14	20.73
I- 584	-14	20.29
I- 585	-14	23.41
I- 586	-14	8.10
I- 587	-14	9.50
I- 588	-15	19.66
I- 589	-15	15.29
I- 590	-15	11.19
I- 591	-16	15.77
I- 592	-16	16.10
I- 593	-16	13.91
I- 594	-17	19.28
I- 595	-17	15.41
I- 596	-17	23.09

APPENDIX A (CONTINUED): D_{Th} AND POSITION AT INVERSAND

Sample Number	Depth relative to basal MFL (cm)	Diameter (mm)
I- 597	-17	14.28
I- 598	-17	5.05
I- 599	-17	14.30
I- 600	-18	14.53
I- 601	-18	14.17
I- 602	-18	17.50
I- 603	-18	16.82
I- 604	-18	9.36
I- 605	-18	9.09
I- 606	-18	17.31
I- 607	-18	7.33
I- 608	-19	12.93
I- 609	-19	14.88
I- 610	-19	13.53
I- 611	-19	13.20
I- 612	-19	8.05
I- 613	-19	8.05
I- 614	-19	14.34
I- 615	-19	15.79
I- 616	-19	11.17
I- 617	-20	15.67
I- 618	-20	12.93
I- 619	-20	7.39
I- 620	-20	19.30
I- 621	-20	9.64
I- 622	-20	13.03
I- 623	-21	11.84
I- 624	-21	13.82
I- 625	-21	19.36
I- 626	-21	11.39
I- 627	-21	17.81
I- 628	-21	16.57
I- 629	-21	16.57
I- 630	-21	14.07
I- 631	-21	13.99

APPENDIX A (CONTINUED): D_{Th} AND POSITION AT INVERSAND

Sample Number	Depth relative to basal MFL (cm)	Diameter (mm)
I- 632	-21	20.81
I- 633	-22	14.82
I- 634	-22	19.23
I- 635	-22	18.77
I- 636	-22	19.70
I- 637	-23	21.59
I- 638	-23	7.83
I- 639	-23	17.07
I- 640	-23	13.63
I- 641	-23	12.37
I- 642	-23	13.18
I- 643	-23	7.03
I- 644	-24	16.15
I- 645	-24	10.24
I- 646	-24	14.43
I- 647	-24	16.96
I- 648	-24	7.01
I- 649	-24	16.83
I- 650	-25	17.11
I- 651	-25	21.33
I- 652	-25	18.23
I- 653	-25	19.01
I- 654	-25	10.41
I- 655	-25	11.09
I- 656	-25	18.58
I- 657	-25	17.68
I- 658	-26	9.94
I- 659	-26	12.20
I- 660	-26	10.78
I- 661	-27	22.01
I- 662	-27	20.46
I- 663	-28	11.79
I- 664	-28	12.56
I- 665	-28	18.25

APPENDIX A (CONTINUED): D_{Th} AND POSITION AT INVERSAND

Sample Number	Depth relative to basal MFL (cm)	Diameter (mm)
I- 666	-29	14.73
I- 667	-29	18.90
I- 668	-29	20.29
I- 669	-29	15.76
I- 670	-29	21.87
I- 671	-29	13.38
I- 672	-29	8.52
I- 673	-30	18.80
I- 674	-30	13.82
I- 675	-30	11.15
I- 676	-30	16.20
I- 677	-30	18.01
I- 678	-30	13.32
I- 679	-30	14.53
I- 680	-30	19.21
I- 681	-30	11.48
I- 682	-31	8.23
I- 683	-31	19.89
I- 701	-35	18.94
I- 702	-35	11.36
I- 703	-35	15.55
I- 704	-35	18.12
I- 705	-35	15.25
I- 706	-36	23.37
I- 707	-37	14.83
I- 708	-37	26.88
I- 709	-37	19.38
I- 710	-37	18.33
I- 711	-37	9.53
I- 712	-38	14.83
I- 713	-38	18.01
I- 714	-38	19.89
I- 715	-38	25.36
I- 716	-38	20.77
I- 717	-39	10.22

APPENDIX A (CONTINUED): D_{Th} AND POSITION AT INVERSAND

Sample Number	Depth relative to basal MFL (cm)	Diameter (mm)
I- 718	-39	12.35
I- 719	-39	9.32
I- 720	-39	7.41
I- 721	-40	12.40
I- 722	-40	17.83
I- 723	-40	17.46
I- 724	-40	11.43
I- 725	-40	16.73
I- 726	-40	15.78
I- 727	-41	11.61
I- 728	-41	10.06
I- 729	-41	28.93
I- 730	-41	5.67
I- 731	-41	15.45
I- 732	-41	14.99
I- 733	-41	11.40
I- 734	-41	11.91
I- 735	-42	10.80
I- 736	-42	15.49
I- 737	-42	15.33
I- 738	-42	9.68
I- 739	-42	12.57
I- 740	-43	15.52
I- 741	-43	10.03
I- 742	-44	17.48
I- 743	-44	26.21
I- 744	-45	18.24
I- 745	-45	22.64
I- 746	-45	20.61
I- 747	-46	25.61
I- 748	-46	16.08
I- 749	-46	15.24
I- 750	-47	17.33
I- 751	-47	25.17
I- 752	-48	20.06

APPENDIX A (CONTINUED): D_{Th} AND POSITION AT INVERSAND

Sample Number	Depth relative to basal MFL (cm)	Diameter (mm)
I- 753	-48	13.46
I- 754	-48	12.94
I- 755	-49	24.46
I- 756	-49	14.53
I- 757	-49	18.18
I- 758	-49	13.35
I- 759	-50	16.33
I- 760	-50	20.88
I- 761	-50	8.48
I- 762	-50	15.51
I- 763	-50	22.52
I- 764	-50	11.55
I- 765	-50	21.72
I- 766	-51	10.54
I- 767	-51	12.40
I- 768	-51	11.66
I- 769	-51	11.20
I- 770	-51	10.15
I- 771	-51	8.37
I- 772	-51	14.03
I- 773	-52	14.53
I- 774	-52	14.96
I- 775	-52	19.17
I- 776	-52	17.50
I- 777	-52	11.07
I- 778	-53	19.15
I- 779	-53	18.72
I- 780	-54	15.49
I- 781	-54	13.63
I- 782	-54	10.49
I- 783	-54	16.24
I- 784	-55	15.75
I- 785	-55	21.39
I- 786	-55	13.27
I- 787	-55	11.71

APPENDIX A (CONTINUED): D_{Th} AND POSITION AT INVERSAND

Sample Number	Depth relative to basal MFL (cm)	Diameter (mm)
I- 788	-55	15.67
I- 789	-56	19.05
I- 790	-56	14.92
I- 791	-56	13.37
I- 792	-57	12.76
I- 793	-57	25.54
I- 794	-57	22.37
I- 795	-58	16.47
I- 796	-58	14.81
I- 797	-58	18.33
I- 798	-59	17.32
I- 799	-59	16.94
I- 800	-59	14.15
I- 801	-59	10.02
I- 802	-59	18.91
I- 803	-59	10.28
I- 804	-59	14.89
I- 805	-59	12.62
I- 806	-60	18.48
I- 807	-60	15.51
I- 808	-60	20.43
I- 809	-60	16.66
I- 810	-61	17.53
I- 811	-61	29.33
I- 812	-61	14.55
I- 813	-61	14.71
I- 814	-62	10.13
I- 815	-62	14.38
I- 816	-62	6.87
I- 817	-63	17.70
I- 818	-63	15.62
I- 819	-63	13.31
I- 820	-64	16.98
I- 821	-64	25.32
I- 822	-64	13.88

APPENDIX A (CONTINUED): D_{Th} AND POSITION AT INVERSAND

Sample Number	Depth relative to basal MFL (cm)	Diameter (mm)
I- 823	-65	14.53
I- 824	-65	11.58
I- 825	-66	15.39
I- 826	-66	27.88
I- 827	-66	15.86
I- 828	-67	18.26
I- 829	-67	14.12
I- 830	-67	14.16
I- 831	-68	17.53
I- 832	-68	17.88
I- 833	-68	15.68
I- 834	-69	15.89
I- 835	-69	7.87
I- 836	-69	12.23
I- 837	-70	14.22
I- 838	-70	19.84
I- 839	-70	16.97
I- 840	-70	12.85
I- 841	-70	14.32
I- 842	-70	12.63
I- 843	-71	12.90
I- 844	-71	15.59
I- 845	-71	12.73
I- 846	-72	20.37
I- 847	-72	20.56
I- 848	-72	9.89
I- 849	-72	6.52
I- 850	-73	9.91
I- 851	-73	15.01
I- 852	-73	11.60
I- 853	-73	16.56
I- 854	-74	5.47
I- 855	-74	11.48
I- 856	-75	13.54
I- 857	-76	14.06

APPENDIX A (CONTINUED): D_{Th} AND POSITION AT INVERSAND

Sample Number	Depth relative to basal MFL(cm)	Diameter (mm)
I- 858	-76	10.35
I- 859	-76	14.88
I- 860	-76	14.74
I- 861	-76	13.28
I- 862	-77	16.48
I- 863	-77	12.55
I- 864	-79	16.42
I- 865	-80	11.13
I- 866	-80	19.99
I- 867	-80	10.09
I- 868	-80	19.91
I- 869	-81	15.57
I- 870	-82	8.04
I- 871	-83	11.25
I- 872	-84	12.89
I- 873	-84	14.72
I- 874	-84	14.02
I- 875	-86	12.56
I- 876	-88	21.18
I- 877	-89	20.05
I- 878	-90	18.26
I- 879	-90	9.12
I- 880	-91	8.37
I- 881	-92	24.21

APPENDIX B: D_{Th} AND POSITION AT RANCOCAS

Sample Number	Depth relative to basal MFL (cm)	Diameter (mm)
R- 1	91	11.61
R- 2	90	8.43
R- 3	90	10.37
R- 4	90	11.87
R- 5	89	10.65
R- 6	87	11.31
R- 7	87	9.47
R- 8	87	11.84
R- 9	86	8.51
R- 10	86	6.72
R- 11	86	9.90
R- 12	86	9.01
R- 13	85	11.26
R- 14	85	7.38
R- 15	85	8.63
R- 16	84	14.07
R- 17	84	7.49
R- 18	84	9.65
R- 19	82	11.25
R- 20	82	14.22
R- 21	81	10.19
R- 22	81	7.75
R- 23	81	18.28
R- 24	81	7.72
R- 25	80	11.43
R- 26	80	13.97
R- 27	79	11.15
R- 28	78	6.33
R- 29	77	12.45
R- 30	76	9.55
R- 31	76	18.03
R- 32	76	10.74
R- 33	76	14.62
R- 34	75	11.89
R- 35	75	11.15

APPENDIX B (CONTINUED): D_{Th} AND POSITION AT RANCOCAS

Sample Number	Depth relative to basal MFL (cm)	Diameter (mm)
R- 36	75	9.70
R- 37	75	12.94
R- 38	75	7.30
R- 39	74	14.20
R- 40	73	16.36
R- 41	73	8.10
R- 42	72	15.82
R- 43	72	7.37
R- 44	71	16.51
R- 45	71	9.65
R- 46	71	11.72
R- 47	70	12.19
R- 48	70	16.23
R- 49	70	13.19
R- 50	69	16.38
R- 51	69	9.12
R- 52	68	7.52
R- 53	68	13.97
R- 54	66	13.74
R- 55	65	14.76
R- 56	65	12.47
R- 57	65	13.89
R- 58	65	9.75
R- 59	64	8.48
R- 60	64	12.61
R- 61	63	9.89
R- 62	62	15.72
R- 63	62	11.81
R- 64	61	10.77
R- 65	61	14.07
R- 66	61	13.26
R- 67	61	11.33
R- 68	60	13.34
R- 69	60	13.97
R- 70	60	10.52

APPENDIX B (CONTINUED): D_{Th} AND POSITION AT RANCOCAS

Sample Number	Depth relative to basal MFL (cm)	Diameter (mm)
R- 71	60	10.33
R- 72	60	7.03
R- 73	59	9.42
R- 74	59	9.09
R- 75	58	15.04
R- 76	57	12.93
R- 77	57	12.75
R- 78	57	11.61
R- 79	56	10.80
R- 80	56	13.97
R- 81	56	10.19
R- 82	56	13.82
R- 83	56	9.14
R- 84	56	5.92
R- 85	56	10.72
R- 86	55	9.96
R- 87	55	16.47
R- 88	55	12.91
R- 89	55	7.96
R- 90	55	10.62
R- 91	55	9.08
R- 92	55	13.45
R- 93	54	11.30
R- 94	54	11.81
R- 95	54	13.84
R- 96	54	7.82
R- 97	54	11.27
R- 98	54	11.88
R- 99	54	11.92
R- 100	54	13.06
R- 101	53	10.05
R- 102	52	10.13
R- 103	52	15.04
R- 104	52	8.20
R- 105	52	15.46

APPENDIX B (CONTINUED): D_{Th} AND POSITION AT RANCOCAS

Sample Number	Depth relative to basal MFL (cm)	Diameter (mm)
R- 106	52	12.62
R- 107	52	10.75
R- 108	51	9.19
R- 109	51	9.34
R- 110	51	15.94
R- 111	51	9.83
R- 112	51	5.08
R- 113	51	10.69
R- 114	50	10.67
R- 115	50	8.94
R- 116	50	16.00
R- 117	50	11.6
R- 118	50	11.06
R- 119	50	13.60
R- 120	50	6.74
R- 121	50	13.77
R- 122	49	13.79
R- 123	49	11.43
R- 124	49	8
R- 125	49	6.7
R- 126	49	8.75
R- 127	49	20.66
R- 128	49	10.48
R- 129	49	6.64
R- 130	49	11.07
R- 131	48	12.29
R- 132	48	11.68
R- 133	48	5.7
R- 134	48	16.65
R- 135	48	10.42
R- 136	47	9.65
R- 137	47	9.12
R- 138	47	10.54
R- 139	47	7.06
R- 140	47	12.71

APPENDIX B (CONTINUED): D_{Th} AND POSITION AT RANCOCAS

Sample Number	Depth relative to basal MFL (cm)	Diameter (mm)
R- 141	46	6.86
R- 142	46	9
R- 143	46	12.42
R- 144	46	10.16
R- 145	45	12.07
R- 146	45	14.00
R- 147	45	9.3
R- 148	45	8.1
R- 149	45	9.55
R- 150	45	10.13
R- 151	45	14.26
R- 152	45	10.11
R- 153	44	14.33
R- 154	44	11.71
R- 155	44	7.7
R- 156	44	9.7
R- 157	44	9.71
R- 158	44	8.72
R- 159	44	8.88
R- 160	43	8.8
R- 161	43	10.3
R- 162	43	7.9
R- 163	43	13.7
R- 164	43	9.2
R- 165	43	8.59
R- 166	42	15.47
R- 167	42	7.6
R- 168	42	5.5
R- 169	42	14.89
R- 170	42	5.64
R- 171	42	6.59
R- 172	42	9.27
R- 173	41	9.53
R- 174	41	14.73
R- 175	41	8.48

APPENDIX B (CONTINUED): D_{Th} AND POSITION AT RANCOCAS

Sample Number	Depth relative to basal MFL (cm)	Diameter (mm)
R- 176	41	9.6
R- 177	41	12.76
R- 178	40	15.34
R- 179	40	14.91
R- 180	40	13.34
R- 181	40	8.1
R- 182	40	9.21
R- 183	39	6.99
R- 184	39	13.36
R- 185	39	14.6
R- 186	39	13.70
R- 187	39	11.47
R- 188	38	13.31
R- 189	38	9.65
R- 190	38	14.22
R- 191	38	12.19
R- 192	38	12.55
R- 193	38	8.4
R- 194	38	9.6
R- 195	38	10.1
R- 196	38	12.11
R- 197	37	8.13
R- 198	37	9.86
R- 199	37	14.02
R- 200	37	13.87
R- 201	36	11.4
R- 202	36	10.02
R- 203	36	15.09
R- 204	36	5.62
R- 205	35	13.84
R- 206	35	14.07
R- 207	35	11.13
R- 208	35	10.98
R- 209	35	7.37
R- 210	34	5.98

APPENDIX B (CONTINUED): D_{Th} AND POSITION AT RANCOCAS

Sample Number	Depth relative to basal MFL (cm)	Diameter (mm)
R- 211	34	9.36
R- 212	34	7.32
R- 213	33	12.32
R- 214	33	15.47
R- 215	33	9.14
R- 216	33	10.3
R- 217	33	16.9
R- 218	33	10.94
R- 219	33	10.23
R- 220	33	9.90
R- 221	32	9.2
R- 222	32	10.3
R- 223	32	8.8
R- 224	32	7.2
R- 225	32	12.19
R- 226	32	14.14
R- 227	31	11.43
R- 228	31	15.47
R- 229	31	16.9
R- 230	31	8.8
R- 231	31	5.30
R- 232	31	12.76
R- 233	30	8.41
R- 234	30	11.76
R- 235	30	9.3
R- 236	30	8.9
R- 237	30	6
R- 238	30	6.4
R- 239	30	11.93
R- 240	29	9.40
R- 241	29	8.51
R- 242	29	14.22
R- 243	29	13.21
R- 244	29	5.5
R- 245	29	8

APPENDIX B (CONTINUED): D_{Th} AND POSITION AT RANCOCAS

Sample Number	Depth relative to basal MFL (cm)	Diameter (mm)
R- 246	29	11.71
R- 247	28	15
R- 248	28	7.3
R- 249	27	10.92
R- 250	27	8.91
R- 251	26	6.68
R- 252	26	6.50
R- 253	26	6
R- 254	26	7.7
R- 255	26	8.7
R- 256	26	7.4
R- 257	26	5.6
R- 258	25	7.75
R- 259	25	14.76
R- 260	25	9.64
R- 261	24	10.21
R- 262	24	6.8
R- 263	23	14.10
R- 264	23	6.6
R- 265	22	8.51
R- 266	22	11.05
R- 267	22	14.73
R- 268	22	21
R- 269	21	8.03
R- 270	21	11.3
R- 271	21	8.1
R- 272	21	18
R- 273	21	19.19
R- 274	20	13.08
R- 275	20	10.06
R- 276	20	14.20
R- 277	20	9.5
R- 278	20	6.8
R- 279	20	5.9
R- 280	20	7.6

APPENDIX B (CONTINUED): D_{Th} AND POSITION AT RANCOCAS

Sample Number	Depth relative to basal	
	MFL (cm)	Diameter (mm)
R- 281	20	16.3
R- 282	20	14.7
R- 283	20	14.68
R- 284	20	6.62
R- 285	19	15.11
R- 286	19	13.89
R- 287	19	19.94
R- 288	19	8.79
R- 289	19	11.6
R- 290	19	10.6
R- 291	19	8.85
R- 292	18	12.45
R- 293	18	10.97
R- 294	18	7.8
R- 295	18	14.8
R- 296	18	15.10
R- 297	17	9.50
R- 298	17	5.9
R- 299	17	8.5
R- 300	17	4.9
R- 301	17	18.9
R- 302	16	13.00
R- 303	16	10.92
R- 304	16	20.09
R- 305	15	15.37
R- 306	15	15.37
R- 307	15	23.62
R- 308	15	17.6
R- 309	15	8
R- 310	15	16.5
R- 311	15	18.6
R- 312	15	16.8
R- 313	14	13.84
R- 314	14	10.5
R- 315	13	10.6

APPENDIX B (CONTINUED): D_{Th} AND POSITION AT RANCOCAS

Sample Number	Depth relative to basal MFL (cm)	Diameter (mm)
R- 316	13	10.40
R- 317	12	22.45
R- 318	12	13.49
R- 319	12	12
R- 320	12	25.9
R- 321	12	7.7
R- 322	12	11.7
R- 323	12	10.1
R- 324	11	18.67
R- 325	11	14.20
R- 326	11	25.6
R- 327	11	19.4
R- 328	11	9.6
R- 329	11	10.7
R- 330	10	17.75
R- 331	10	15.11
R- 332	10	8.6
R- 333	10	8
R- 334	10	15.8
R- 335	10	9.1
R- 336	10	12.7
R- 337	10	17.5
R- 338	10	12.09
R- 339	9	14.22
R- 340	9	11.68
R- 341	9	16.64
R- 342	9	16.26
R- 343	9	19.53
R- 344	9	22.8
R- 345	9	11.4
R- 346	9	12.6
R- 347	9	12.58
R- 348	8	17.27
R- 349	8	13.46
R- 350	8	13.74

APPENDIX B (CONTINUED): D_{Th} AND POSITION AT RANCOCAS

Sample Number	Depth relative to basal MFL (cm)	Diameter (mm)
R- 351	8	18.21
R- 352	8	4.34
R- 353	7	16.64
R- 354	7	13.34
R- 355	7	9.3
R- 356	7	11.10
R- 357	6	18.29
R- 358	6	10.92
R- 359	6	12.73
R- 360	6	9.04
R- 361	6	13.4
R- 362	6	10.7
R- 363	6	10.2
R- 364	6	15.8
R- 365	6	15.80
R- 366	6	5.54
R- 367	5	26.04
R- 368	5	18.85
R- 369	5	12.9
R- 370	5	12.6
R- 371	5	8.43
R- 372	5	14.10
R- 373	4	19.66
R- 374	4	10.01
R- 375	4	23.65
R- 376	4	17.17
R- 377	4	12
R- 378	4	17.3
R- 379	4	17.20
R- 380	3	17.53
R- 381	3	8.7
R- 382	3	13.49
R- 383	2	14.50
R- 384	2	19.15
R- 385	2	11.8

APPENDIX B (CONTINUED): D_{Th} AND POSITION AT RANCOCAS

Sample Number	Depth relative to basal MFL (cm)	Diameter (mm)
R- 386	2	9.33
R- 387	1	8.38
R- 388	1	18.59
R- 389	1	14.4
R- 390	1	10.7
R- 391	1	18.8
R- 392	0	23.29
R- 393	0	4.4
R- 394	0	15.56
R- 395	0	11.11
R- 396	-1	16.64
R- 397	-1	15.22
R- 398	-2	15.47
R- 399	-2	25.15
R- 400	-2	16.2
R- 401	-3	18.16
R- 402	-3	17.65
R- 403	-3	11.11
R- 404	-4	15.27
R- 405	-4	13.46
R- 406	-4	9.14
R- 407	-5	15.98
R- 408	-5	18.77
R- 409	-5	13.23
R- 410	-6	18.54
R- 411	-6	20.70
R- 412	-6	13.69
R- 413	-7	12.67
R- 414	-7	17.7
R- 415	-7	13.4
R- 416	-8	15.11
R- 417	-8	15.9
R- 418	-8	9.42
R- 419	-8	12.49
R- 420	-9	22.48

APPENDIX B (CONTINUED): D_{Th} AND POSITION AT RANCOCAS

Sample Number	Depth relative to basal MFL (cm)	Diameter (mm)
R- 421	-9	16.28
R- 422	-9	19.46
R- 423	-9	12.4
R- 424	-9	11.6
R- 425	-9	11.84
R- 426	-9	14.79
R- 427	-10	18.67
R- 428	-10	9.9
R- 429	-10	5.62
R- 430	-10	7.19
R- 431	-11	18.67
R- 432	-11	17.5
R- 433	-11	11.02
R- 434	-12	16.23
R- 435	-12	10.02
R- 436	-12	8.24
R- 437	-12	12.54
R- 438	-12	11.12
R- 439	-13	13.2
R- 440	-13	9.9
R- 441	-13	13.9
R- 442	-13	13.65
R- 443	-14	11.7
R- 444	-15	15.82
R- 445	-15	19.86
R- 446	-15	13.34
R- 447	-15	27.9
R- 448	-15	18.36
R- 449	-15	11.24
R- 450	-15	10.25
R- 451	-16	24.38
R- 452	-16	5.21
R- 453	-16	17.71
R- 454	-16	12.41
R- 455	-17	12.2

APPENDIX B (CONTINUED): D_{Th} AND POSITION AT RANCOCAS

Sample Number	Depth relative to basal MFL (cm)	Diameter (mm)
R- 456	-17	8.70
R- 457	-17	18.37
R- 458	-18	17.13
R- 459	-18	17.94
R- 460	-19	15.62
R- 461	-19	23.1
R- 462	-20	20.70
R- 463	-20	11.81
R- 464	-20	23.52
R- 465	-20	26.9
R- 466	-21	13.06
R- 467	-21	10.93
R- 468	-21	12.65
R- 469	-21	15.20
R- 470	-21	9.91
R- 471	-22	16.13
R- 472	-22	16.38
R- 473	-23	18.42
R- 474	-23	15.52
R- 475	-23	31.4
R- 476	-24	28.09
R- 477	-24	15.11
R- 478	-24	14.00
R- 479	-25	14.81
R- 480	-25	13.69
R- 481	-25	15.85
R- 482	-26	24.8
R- 483	-26	15
R- 484	-26	12.99
R- 485	-27	13.44
R- 486	-27	22.23
R- 487	-27	12.40
R- 488	-28	22.48
R- 489	-28	10.97
R- 490	-28	14.00

APPENDIX B (CONTINUED): D_{Th} AND POSITION AT RANCOCAS

Sample Number	Depth relative to basal MFL (cm)	Diameter (mm)
R- 491	-29	18.29
R- 492	-29	8.15
R- 493	-29	10.84
R- 494	-30	17.53
R- 495	-30	14
R- 496	-30	14.46
R- 497	-31	13.87
R- 498	-32	18.57
R- 499	-32	23.65
R- 500	-32	16.89
R- 501	-34	8.89
R- 502	-34	9.34
R- 503	-35	17.07
R- 504	-35	13.27
R- 505	-36	13.23
R- 506	-36	19.52
R- 507	-37	31.80
R- 508	-38	16.51
R- 509	-38	10.29
R- 510	-39	17.37
R- 511	-39	11.00
R- 512	-43	23.55
R- 513	-43	10.80
R- 514	-44	12.13
R- 515	-48	18.39
R- 516	-50	13.23
R- 517	-54	21.67
R- 518	-56	14.31
R- 519	-58	14.81
R- 520	-59	15.11
R- 521	-60	22.58
R- 522	-60	20.70
R- 523	-60	16.23
R- 524	-61	27.08
R- 525	-61	13.44

APPENDIX B (CONTINUED): D_{Th} AND POSITION AT RANCOCAS

Sample Number	Depth relative to basal MFL (cm)	Diameter (mm)
R- 526	-62	15.37
R- 527	-65	13.41
R- 528	-66	16.99
R- 529	-68	11.40
R- 530	-69	19.08
R- 531	-70	12.50
R- 532	-71	17.02
R- 533	-71	13.59
R- 534	-71	6.73
R- 535	-72	16.71
R- 536	-72	15.90
R- 537	-72	12.03
R- 538	-73	15.62
R- 539	-73	18.64
R- 540	-73	13.84
R- 541	-73	22.73
R- 542	-73	12.82
R- 543	-74	11.37
R- 544	-75	13.50
R- 545	-78	16.36
R- 546	-78	12.83
R- 547	-79	20.83
R- 548	-79	12.46
R- 549	-80	14.00
R- 550	-80	21.31
R- 551	-82	11.56
R- 552	-86	9.42
R- 553	-87	20.22
R- 554	-88	20.37
R- 555	-89	11.89
R- 556	-89	23.34
R- 557	-89	24.18
R- 558	-90	18.03
R- 559	-91	17.65
R- 560	-92	17.91

APPENDIX B (CONTINUED): D_{Th} AND POSITION AT RANCOCAS

Sample Number	Depth relative to basal MFL (cm)	Diameter (mm)
R- 561	-94	25.63
R- 562	-94	6.73
R- 563	-95	15.75
R- 564	-95	10.39
R- 565	-97	20.80
R- 566	-98	22.48
R- 567	-99	18.14
R- 568	-101	27.58
R- 569	-102	18.03
R- 570	-103	24.23
R- 571	-104	15.34
R- 572	-106	14.50
R- 573	-106	7.98
R- 574	-109	20.80
R- 575	-109	17.65
R- 576	-111	16.00
R- 577	-111	12.98
R- 578	-112	26.95

APPENDIX C: D_{Th} AND STRATIGRAPHIC POSITION AT WALNRIDGE

Sample Number	Depth relative to Navesink/Hornerstown contact (cm)	Diameter (mm)
W- 1	141	13.46
W- 2	140	12.50
W- 3	137	12.70
W- 4	136	10.54
W- 5	134	13.84
W- 6	131	12.75
W- 7	130	7.85
W- 8	128	6.99
W- 9	127	16.76
W- 10	126	12.80
W- 11	126	14.73
W- 12	124	7.59
W- 13	123	14.48
W- 14	119	12.14
W- 15	119	14.83
W- 16	119	6.15
W- 17	118	18.08
W- 18	118	14.25
W- 19	110	14.38
W- 20	109	8.41
W- 21	109	8.43
W- 22	108	13.72
W- 23	108	10.90
W- 24	107	11.81
W- 25	106	15.21
W- 26	106	11.94
W- 27	105	12.42
W- 28	105	11.91
W- 29	104	11.81
W- 30	104	15.49
W- 31	103	12.90
W- 32	102	14.71
W- 33	101	16.28
W- 34	100	13.44
W- 35	100	15.98

APPENDIX C (CONTINUED): D_{Th} AND POSITION AT WALNRIDGE

Sample Number	Depth relative to Navesink/Hornerstown contact (cm)	Diameter (mm)
W- 36	100	7.42
W- 37	99	6.45
W- 38	99	13.11
W- 39	99	15.19
W- 40	98	12.50
W- 41	97	8.41
W- 42	95	14.78
W- 43	95	10.54
W- 44	95	9.98
W- 45	95	8.84
W- 46	94	12.88
W- 47	94	6.38
W- 48	92	14.50
W- 49	91	13.49
W- 50	90	14.63
W- 51	90	13.28
W- 52	89	11.84
W- 53	88	12.52
W- 54	88	9.02
W- 55	88	9.98
W- 56	87	11.13
W- 57	85	13.44
W- 58	85	12.55
W- 59	85	11.10
W- 60	84	9.78
W- 61	84	16.59
W- 62	83	13.11
W- 63	83	9.19
W- 64	82	8.26
W- 65	82	10.92
W- 66	82	13.34
W- 67	81	15.24
W- 68	81	7.87
W- 69	81	14.02
W- 70	80	11.66

APPENDIX C (CONTINUED): D_{Th} AND POSITION AT WALNRIDGE

Sample Number	Depth relative to Navesink/Hornerstown contact (cm)	Diameter (mm)
W- 71	80	10.26
W- 72	80	14.07
W- 73	78	16.89
W- 74	78	14.45
W- 75	78	11.89
W- 76	77	12.42
W- 77	76	8.84
W- 78	76	6.71
W- 79	76	13.54
W- 80	75	12.01
W- 81	75	10.01
W- 82	74	8.84
W- 83	72	13.51
W- 84	70	16.21
W- 85	69	14.33
W- 86	69	10.24
W- 87	69	6.73
W- 88	68	11.68
W- 89	68	12.37
W- 90	66	9.42
W- 91	65	13.45
W- 92	65	6.76
W- 93	64	8.66
W- 94	64	12.83
W- 95	64	16.22
W- 96	63	11.84
W- 97	63	12.57
W- 98	63	14.81
W- 99	62	12.45
W- 100	62	13.46
W- 101	62	10.03
W- 102	62	12.47
W- 103	61	10.57
W- 104	61	13.49
W- 105	59	8.26

APPENDIX C (CONTINUED): D_{Th} AND POSITION AT WALNRIDGE

Sample Number	Depth relative to Navesink/Hornerstown contact (cm)	Diameter (mm)
W- 106	59	13.52
W- 107	58	9.40
W- 108	58	16.46
W- 109	57	12.83
W- 110	57	10.66
W- 111	57	13.48
W- 112	56	11.18
W- 113	56	13.72
W- 114	56	11.05
W- 115	55	13.34
W- 116	55	10.92
W- 117	55	12.22
W- 118	53	14.73
W- 119	53	17.65
W- 120	52	16.03
W- 121	52	9.02
W- 122	51	8.61
W- 123	50	14.73
W- 124	50	10.52
W- 125	49	12.17
W- 126	49	8.51
W- 127	49	13.20
W- 128	48	9.30
W- 129	48	15.62
W- 130	48	8.92
W- 131	48	9.50
W- 132	47	13.84
W- 133	47	13.03
W- 134	47	9.02
W- 135	46	6.58
W- 136	45	13.26
W- 137	45	14.14
W- 138	44	12.70
W- 139	44	7.33
W- 140	43	13.82

APPENDIX C (CONTINUED): D_{Th} AND POSITION AT WALNRIDGE

Sample Number	Depth relative to Navesink/Hornerstown contact (cm)	Diameter (mm)
W- 141	43	16.83
W- 142	42	12.07
W- 143	42	9.80
W- 144	42	5.59
W- 145	42	10.54
W- 146	41	17.04
W- 147	41	5.09
W- 148	41	8.08
W- 149	41	3.86
W- 150	40	15.72
W- 151	40	16.13
W- 152	40	10.46
W- 153	40	5.96
W- 154	39	14.48
W- 155	39	4.60
W- 156	39	6.32
W- 157	39	9.51
W- 158	38	17.27
W- 159	38	13.44
W- 160	38	14.80
W- 161	37	15.11
W- 162	37	13.84
W- 163	37	15.54
W- 164	37	13.69
W- 165	37	13.67
W- 166	36	9.07
W- 167	35	12.57
W- 168	35	9.75
W- 169	35	7.54
W- 170	35	14.30
W- 171	34	16.08
W- 172	34	7.19
W- 173	33	10.54
W- 174	33	6.65
W- 175	33	6.10

APPENDIX C (CONTINUED): D_{Th} AND POSITION AT WALNRIDGE

Sample Number	Depth relative to Navesink/Hornerstown contact (cm)	Diameter (mm)
W- 176	33	14.15
W- 177	32	13.15
W- 178	31	8.51
W- 179	31	10.61
W- 180	30	8.64
W- 181	30	14.66
W- 182	30	6.58
W- 183	30	11.20
W- 184	29	12.45
W- 185	29	16.59
W- 186	29	12.93
W- 187	29	18.11
W- 188	28	20.65
W- 189	25	9.37
W- 190	25	12.88
W- 191	24	9.14
W- 192	24	10.67
W- 193	22	15.01
W- 194	22	13.90
W- 195	21	8.43
W- 196	21	8.32
W- 197	20	20.45
W- 198	20	13.03
W- 199	20	18.08
W- 200	20	9.17
W- 201	20	9.88
W- 202	19	10.96
W- 203	19	17.10
W- 204	18	9.92
W- 205	18	5.71
W- 206	17	18.92
W- 207	17	12.55
W- 208	16	14.02
W- 209	16	18.08
W- 210	15	9.45

APPENDIX C (CONTINUED): D_{Th} AND POSITION AT WALNRIDGE

Sample Number	Depth relative to Navesink/Hornerstown contact (cm)	Diameter (mm)
W- 211	15	13.21
W- 212	14	16.38
W- 213	14	14.00
W- 214	14	18.82
W- 215	14	13.56
W- 216	14	16.03
W- 217	13	13.46
W- 218	13	11.63
W- 219	13	19.80
W- 220	12	19.94
W- 221	12	13.54
W- 222	11	18.54
W- 223	11	22.61
W- 224	11	16.27
W- 225	10	9.60
W- 226	9	12.83
W- 227	8	24.05
W- 228	8	15.95
W- 229	4	8.71
W- 230	4	14.10
W- 231	3	20.02
W- 232	3	20.70
W- 233	1	21.69
W- 234	1	13.93
W- 235	0	21.21
W- 236	0	14.71
W- 237	-3	18.03
W- 238	-8	16.00
W- 239	-9	9.52
W- 240	-10	6.89
W- 241	-10	10.76
W- 242	-11	15.57
W- 243	-11	9.24
W- 244	-12	11.04
W- 245	-13	18.31

APPENDIX C (CONTINUED): D_{Th} AND POSITION AT WALNRIDGE

Sample Number	Depth relative to Navesink/Hornerstown contact (cm)	Diameter (mm)
W- 246	-15	15.88
W- 247	-15	19.28
W- 248	-17	17.12
W- 249	-19	11.96
W- 250	-20	13.46
W- 251	-25	17.50
W- 252	-26	14.02
W- 253	-27	9.53
W- 254	-28	10.64
W- 255	-32	18.01
W- 256	-32	23.11
W- 257	-33	13.84
W- 258	-34	19.71
W- 259	-37	23.27
W- 260	-39	20.35
W- 261	-39	13.72
W- 262	-40	16.03
W- 263	-41	18.29
W- 264	-42	19.58
W- 265	-42	18.42
W- 266	-43	25.68
W- 267	-44	20.17
W- 268	-45	21.21
W- 269	-46	24.00
W- 270	-46	14.07
W- 271	-47	26.80
W- 272	-48	12.19
W- 273	-49	23.55
W- 274	-50	21.49
W- 275	-52	24.89
W- 276	-60	20.55
W- 277	-60	24.77
W- 278	-60	16.89
W- 279	-62	20.98
W- 280	-63	10.95

APPENDIX C (CONTINUED): D_{Th} AND POSITION AT WALNRIDGE

Sample Number	Depth relative to Navesink/Hornerstown contact (cm)	Diameter (mm)
W- 281	-65	15.49
W- 282	-69	18.80
W- 283	-71	12.98
W- 284	-73	17.65
W- 285	-76	22.86
W- 286	-78	20.32
W- 287	-78	15.88
W- 288	-80	23.09
W- 289	-82	19.05
W- 290	-89	25.12
W- 291	-90	17.25
W- 292	-92	22.53
W- 293	-95	14.45
W- 294	-96	17.42
W- 295	-98	12.29
W- 296	-99	14.99
W- 297	-101	6.60
W- 298	-104	9.35
W- 299	-106	11.43
W- 300	-106	20.45
W- 301	-109	15.70
W- 302	-109	20.60
W- 303	-110	13.84
W- 304	-113	13.97
W- 305	-116	18.64
W- 306	-138	13.08
W- 307	-140	23.52
W- 308	-180	18.67

APPENDIX D: D_{Th} AND BED # AT BRAGGS

Bed	Sample	Diameter (mm)	Bed	Sample	Diameter (mm)
B3-	1	16.28	B7-	15	8.78
B3-	2	13.17	B7-	16	7.83
B3-	3	12.96	B7-	17	10.44
B3-	4	9.43	B7-	18	8.97
B3-	5	13.4	B7-	19	9.29
B3-	6	13.29	B7-	20	9.87
B3-	7	11.3	B7-	21	12.8
B3-	8	12.84	B7-	22	10.13
B3-	9	10.61	B7-	23	14.34
B3-	10	14.72	B7-	24	8.94
B3-	11	12.99	B7-	25	11.71
B3-	12	13.39	B7-	26	9.37
B3-	13	16.07			
B3-	14	12.71			

**APPENDIX E: D_{Th} AND UNIT AT BRAZOS RIVER /
COTTONMOUTH CREEK**

Unit- #	Diameter (mm)
A3- 1	36.27
A3- 2	30.18
A3- 3	23.83
A3- 4	13.5
A3- 5	23.29
A3- 6	24.56
A3- 7	15.04
A3- 8	17.36
A3- 9	11.35
A3- 10	27.78
A3- 11	27.12
A3- 12	22.87
A3- 13	20.1
A3- 14	26.66
A3- 15	24.42
A3- 16	19.47
A3- 17	19.59
A3- 18	17.16
A3- 19	18.53
A3- 20	24.7
A3- 21	22.12
A3- 22	21.97
A3- 23	21.63
A3- 24	13.53
A3- 25	17.72
A3- 26	18.02
A3- 27	22.82
A3- 28	20.6
A3- 29	12.55
A3- 30	27.99
A3- 31	28.37
A3- 32	15.28
A3- 33	29.28
A3- 34	12.34
A3- 35	14.71

**APPENDIX E (CONTINUED): D_{Th} AND LITHOLOGIC UNIT AT
BRAZOS RIVER / COTTONMOUTH CREEK**

Unit- #	Diameter (mm)
A3- 36	14.97
A3- 37	22.78
A3- 38	23.56
A3- 39	23.89
A3- 40	22.57
A3- 41	26.2
A3- 42	28.42
HCS- 1	15.62
HCS- 2	13.54
HCS- 3	25.93
HCS- 4	26.19
HCS- 5	15.47
HCS- 6	14.81
HCS- 7	13.6
HCS- 8	18.18
HCS- 9	10.73
HCS- 10	18.43
HCS- 11	13.02
HCS- 12	19.4
HCS- 13	17.92
HCS- 14	15.09
HCS- 15	11.09
HCS- 16	10.07
HCS- 17	13.76
HCS- 18	13.46
HCS- 19	8.73
HCS- 20	17.97
HCS- 21	13.9
HCS- 22	9.86
HCS- 23	10.29
HCS- 24	20.92
HCS- 25	8.36
HCS- 26	14.25
HCS- 27	12.61
HCS- 28	17.57

**APPENDIX E (CONTINUED): D_{Th} AND LITHOLOGIC UNIT AT
BRAZOS RIVER / COTTONMOUTH CREEK**

Unit- #	Diameter (mm)
HCS- 29	12.4
HCS- 30	16.61
HCS- 31	17.21
HCS- 32	16.7
HCS- 33	10.67
HCS- 34	10.31
HCS- 35	17.22
HCS- 36	16.57
HCS- 37	16.96
HCS- 38	12.99
HCS- 39	15.55
HCS- 40	7.93
HCS- 41	6.96
HCS- 42	8.15
HCS- 43	6.8
HCS- 44	13.52
HCS- 45	7.52
HCS- 46	11.43
HCS- 47	9.72
HCS- 48	13.2
HCS- 49	18.85
HCS- 50	15.59
HCS- 51	9.82
HCS- 52	13.3
HCS- 53	13.95
HCS- 54	13.66
HCS- 55	15.46
HCS- 56	8.99
HCS- 57	19.7
HCS- 58	7.91
HCS- 59	15.32
HCS- 60	14.14
HCS- 61	16.73
HCS- 62	7.18
HCS- 63	6.98

**APPENDIX E (CONTINUED): D_{Th} AND LITHOLOGIC UNIT AT
BRAZOS RIVER / COTTONMOUTH CREEK**

Unit- #	Diameter (mm)
HCS- 64	5.99
HCS- 65	8.58
HCS- 66	9.25
HCS- 67	7.19
HCS- 68	12.67
HCS- 69	11.28
HCS- 70	21.19
HCS- 71	10.07
HCS- 72	11.28
HCS- 73	8.94
HCS- 74	9.82
HCS- 75	7.6
HCS- 76	8.43
HCS- 77	6.7
HCS- 78	6.3
HCS- 79	7.06
HCS- 80	7.82
HCS- 81	10.27
HCS- 82	6.59
HCS- 83	14.51
HCS- 84	17.43
HCS- 85	11.4
HCS- 86	10.29
HCS- 87	8.06
HCS- 88	13.6
HCS- 89	10.51
HCS- 90	8.79
HCS- 91	11.45
HCS- 92	8.15
HCS- 93	6.53
E2- 1	18.65
E2- 2	13.44
E2- 3	19.13
E2- 4	7.56
E2- 5	25.92

APPENDIX E (CONTINUED): D_{Th} AND LITHOLOGIC UNIT AT BRAZOS RIVER / COTTONMOUTH CREEK

Unit- #	Diameter (mm)
E2- 6	11.41
E2- 7	26.82
E2- 8	20.14
E2- 9	17.36
E2- 10	15.2
E2- 11	21.39